



# What is the cause(s) of positive ozone trends in three megacity clusters in eastern China during 2015–2020?

Tingting Hu<sup>1</sup>, Yu Lin<sup>1</sup>, Run Liu<sup>1,2</sup>, Yuepeng Xu<sup>1</sup>, Boguang Wang<sup>1,2</sup>, Yuanhang Zhang<sup>3</sup>, Shaw Chen Liu<sup>1,2</sup>

<sup>1</sup>Institute for Environmental and Climate Research, Jinan University, Guangzhou, 511443, China

5 <sup>2</sup>Guangdong-Hongkong-Macau Joint Laboratory of Collaborative Innovation for Environmental Quality, Guangzhou, 511443, China

<sup>3</sup>State Key Joint Laboratory of Environmental Simulation and Pollution Control, College of Environmental Sciences and Engineering, Peking University, Beijing, 100871, China

10 *Correspondence to:* Run Liu (liurun@jnu.edu.cn), Shaw Chen Liu (shawliu@jnu.edu.cn)

**Abstract.** Due to a robust emission control policy, significant reductions in major air pollutants, such as PM<sub>2.5</sub>, SO<sub>2</sub>, NO<sub>2</sub>, and CO, were observed in China between 2015 to 2020. On the other hand, during the same period, there was a notable increase in ozone (O<sub>3</sub>) concentrations, making it a prominent air pollutant in eastern China. The annual mean concentration of maximum daily 8-hour average (MDA8) O<sub>3</sub> exhibited alarming linear trends of 2.4, 1.1, and 2.0 ppb yr<sup>-1</sup> in three megacity clusters: 15 Beijing-Tianjin-Hebei (BTH), Yangtze River Delta (YRD) and Pearl River Delta (PRD). Additionally, there was a significant three-fold increase in the number of O<sub>3</sub>-exceeding days, defined as MDA8 O<sub>3</sub> > 75 ppb during the same period. Our analysis indicated that the upward trends in the annual mean concentration of MDA8 were primarily driven by the rise in consecutive O<sub>3</sub>-exceeding days. Furthermore, from 2015 to 2017, there was a widespread expansion of high O<sub>3</sub> concentrations from urban centers to surrounding rural regions, resulting in a more uniform spatial distribution of O<sub>3</sub> after 2017. Lastly, we discovered a 20 close association between O<sub>3</sub> episodes featuring four or more consecutive O<sub>3</sub>-exceeding days and the position and strength of the West Pacific subtropical high (WPSH). The WPSH contributed to meteorological conditions characterized by clear skies, subsiding air motion, high vertical stability in the lower troposphere, increased solar radiation, and positive temperature anomaly at the surface. These favorable meteorological conditions greatly facilitated the formation of O<sub>3</sub>. Thus, we propose that the worsening O<sub>3</sub> trends observed in BTH, YRD and PRD from 2015 to 2020 can be attributed to enhanced photochemical 25 O<sub>3</sub> production resulting from an increased occurrence of meteorological conditions with high solar radiation and positive temperature anomalies under the influence of WPSH and tropical cyclones.

## 1 Introduction

Ozone (O<sub>3</sub>) is an important greenhouse gas, which can also have adverse effects on human health, vegetation, and materials (Bell et al., 2006; Cohen et al., 2017; Kalabokas et al., 2020; Nuvolone et al., 2018). Surface O<sub>3</sub> is a secondary pollutant 30 produced by photochemical reactions involving O<sub>3</sub> precursors such as volatile organic compounds (VOCs), carbon monoxide (CO) and nitrogen oxides (NO<sub>x</sub>) (Ma et al., 2012; Monks et al., 2015; Wang et al., 2017). Compared to O<sub>3</sub> precursors,



meteorological conditions are also crucial factors driving the O<sub>3</sub> formation. Solar radiation, temperature, relative humidity, wind speed, and cloud cover have been found to be closely related to O<sub>3</sub> formation (Dong et al., 2020; Han et al., 2020; Yin et al., 2019). In addition, large-scale circulations, such as the East Asian monsoon, West Pacific subtropical high (WPSH) and tropical cyclones (TCs) can influence O<sub>3</sub> concentration as well (Lu et al., 2019; Rowlinso et al., 2019; Yang et al., 2014; Zhao and Wang, 2017).

The concentrations of air pollutants SO<sub>2</sub>, NO<sub>x</sub>, CO, PM<sub>10</sub> and PM<sub>2.5</sub> in China have been significantly reduced since 2013 (Li M. et al., 2021; Li et al., 2022; Zhai et al., 2019), thanks to the implementation of “Air Pollution Prevention and Control Action Plan”. However, the O<sub>3</sub> concentration has dramatically increased and emerged as a major air pollutant in eastern China (Bian et al., 2019; Fu et al., 2019; Wang et al., 2020; Zheng et al., 2018). O<sub>3</sub> concentrations are particularly high in the three megacity clusters in eastern China, namely Beijing-Tianjin-Hebei (BTH), Yangtze River Delta (YRD) and Pearl River Delta (PRD) (Gao et al., 2020; Guo et al., 2019; Li K. et al., 2021; Liu et al., 2018; Yang et al., 2019).

Annual mean concentrations of maximum daily 8-hour average (MDA8) O<sub>3</sub> in the three megacity clusters are shown in Fig. 1. The linear increasing trends of MDA8 O<sub>3</sub> for BTH, YRD and PRD are 2.4, 1.1 and 2.0 ppb yr<sup>-1</sup>, respectively during the period 2015–2020. These trends are unusually large compared to the trends in other parts of China as well as the trends worldwide (Chen et al., 2020; Lu et al., 2018; Professional Committee of Ozone Pollution Control of Chinese Society for Environmental Sciences, 2022; Zhang et al., 2020). Thus, a crucial scientific question is: What is the cause(s) of these large positive trends in O<sub>3</sub> concentration? Some recent studies suggested that changing photochemical processes induced by anthropogenic emissions are responsible for these trends (Li et al., 2019; Li et al., 2022; Shao et al., 2021; Wang et al., 2020). However, in our analysis of the O<sub>3</sub> trends at individual stations in eastern China during the period 2015–2020, we noticed that the interannual variations of O<sub>3</sub> concentration were strongly affected by the position and intensity of WPSH and the presence of TCs in the western Pacific and South China Sea, consistent with the results of a number of recent studies (Chang et al., 2019; Mao et al., 2020; Ouyang et al., 2022; Zhao and Wang, 2017). These results suggest that transport/meteorological parameters associated with WPSH and TCs may play an important role in the large trends of MDA8 O<sub>3</sub>.

The significant impact of WPSH on weather patterns and O<sub>3</sub> concentrations over East China is widely recognized (Bachmann, 2015; Chang et al., 2019; Yin et al., 2019; Zhao and Wang, 2017). It is well established that the WPSH plays a critical role in controlling weather conditions, which in turn affects O<sub>3</sub> concentrations. For example, the WPSH is known to contribute to the formation of the East Asian monsoon and influence precipitation patterns in the YRD. Furthermore, it also influences air temperature and precipitation across North and South China (Zhang, 2001; Zhao and Wang, 2017). These changes in meteorological conditions have a profound impact on the photochemical formation, dispersion, and accumulation of O<sub>3</sub>.

Previous studies have indicated that in the outer regions of TCs, PRD experiences specific atmospheric conditions, e.g., high pressure, low humidity, and intense solar radiation. These conditions often result in consecutive days with elevated levels of O<sub>3</sub>, as observed in various case studies (Ouyang et al., 2022; Wei et al., 2016). Furthermore, statistical investigations have established several noteworthy connections between TCs and O<sub>3</sub> concentrations in the PRD area. For example, the meteorological conditions associated with the TC periphery frequently contributed to the formation of elevated surface O<sub>3</sub>



levels and aerosols (Deng et al., 2019). In addition, TCs in the East China Sea had a higher likelihood of causing increased O<sub>3</sub> concentrations in the PRD region (Zhao et al., 2022). Lastly, TCs in the vicinity of Taiwan, China have the greatest influence on air quality in Hong Kong when compared to TCs in other areas, which is primarily because these TCs facilitate the transportation of air pollutants from the PRD region (Lam et al., 2018).

70 In this study, we focus on exploring possible contributions to the large positive O<sub>3</sub> trends in the three megacity clusters in eastern China by changes in meteorological parameters associated with WPSH and TCs during the period 2015–2020. This paper is organized as follows. In Section 2, the data and methodology used in this study are described. Major characteristics of the O<sub>3</sub> interannual variability and trends in the three megacity clusters are discussed in Section 3.1. In Section 3.2, we examine the spatial expansion and quasi-saturation of high O<sub>3</sub>. The annual change of O<sub>3</sub>-exceeding days with different  
75 durations are also examined. A hypothesis of the cause of O<sub>3</sub> trends in three megacity clusters in eastern China during 2015–2020 is presented in Section 3.3. Section 4 presents a summary and conclusions.

## 2 Data and methodology

### 2.1 Pollutant Data

In this study, the observed hourly concentrations of air pollutants, including O<sub>3</sub>, NO<sub>2</sub>, CO, PM<sub>2.5</sub>, and SO<sub>2</sub> from 2015 to 2020  
80 are obtained from the Chinese National Environmental Ministry of Environmental Protection (<http://www.cnemc.cn/en/>). Gridded MDA8 O<sub>3</sub> data from Tracking Air Pollution in China dataset (<http://tapdata.org.cn>) with a resolution of 10 km are also used (Xue et al., 2020).

### 2.2 Meteorological Data

The European Centre for Medium-Range Weather Forecasts (ECMWF) Reanalysis v5 (ERA5) dataset (available at  
85 <https://cds.climate.copernicus.eu/>), with a horizontal resolution of 0.25° × 0.25° and a time interval of 1 h, was used to analyze the influence of meteorological parameters on O<sub>3</sub> pollution. The variables used in this study include 2 m temperature (T2m), surface net solar radiation (SSR). In addition, daily mean relative humidity, geopotential height, zonal and meridional wind at 500 hPa from the National Center for Environmental Prediction (NCEP) and National Center for Atmospheric Research (NCAR) reanalysis (<https://psl.noaa.gov/data/gridded/data.ncep.reanalysis.html>) at a resolution of 2.5° × 2.5° are used.

### 90 2.3 Methods

The Chinese National Ambient Air Quality Standard for MDA8 O<sub>3</sub> is 160 µg m<sup>-3</sup>, which corresponds to 75 ppb at 273.15 K and 1 atm. It follows that the O<sub>3</sub>-exceeding days are defined as MDA8 O<sub>3</sub> concentration >75 ppb, while non-O<sub>3</sub>-exceeding days are defined as MDA8 O<sub>3</sub> concentration <75 ppb. According to the duration of O<sub>3</sub> pollution, it can be divided into consecutive O<sub>3</sub>-exceeding days with four or more days (O<sub>3</sub> days ≥ 4) and consecutive O<sub>3</sub>-exceeding days less than four days



95 ( $O_3$  days $<4$ ). In addition, some common statistical methods are used in this study, including linear fitting, meteorological synthesis method, and two-tailed Student's t test.

The normalized annual mean  $O_3$  concentration of the  $O_3$ -exceeding days is calculated by adding the  $O_3$  concentration of the  $O_3$ -exceeding day each year and dividing it by the total number of days in the year. The normalized annual mean  $O_3$  of the non- $O_3$ -exceeding days is calculated by the same method except for the non- $O_3$ -exceeding days.

100 Table 1 lists the criteria and corresponding numbers of low  $O_3$  and high  $O_3$  stations in the three megacity clusters. Low  $O_3$  and high  $O_3$  stations are defined basing on the number of  $O_3$  exceeding days in 2015. Stations with the number of  $O_3$ -exceeding days fewer than or equal to the low  $O_3$  criterion (second column) are considered as low  $O_3$  stations. When more than or equal to the high  $O_3$  criterion (4<sup>th</sup> column), they are considered as high  $O_3$  stations. We have tested a few reasonably different criteria and found only some insignificant differences in the results. i.e., the results associated with low  $O_3$  and high  $O_3$  stations are  
105 robust against reasonable changes in their selection criteria. For example, the relatively large criterion (37 days) of low  $O_3$  stations in YRD is intended to include a large enough number of stations (about one third of the total of 152 stations) to be fully representative of low  $O_3$  and moderate  $O_3$  stations. These results have been compared to those of a more stringent criterion of nineteen days and found no notable change in the major characteristics (Figs. S1 and S2).

### 3 Results and discussion

#### 110 3.1 Major characteristics of $O_3$ trends

Major characteristics of the large positive trends in the annual mean  $O_3$  concentration are shown in Figs. 2a, 2b and 2c for BTH, YRD and PRD, respectively, in which the normalized annual mean concentrations of MDA8  $O_3$  in the three megacity clusters are compared to contributions from two groups: The  $O_3$ -exceeding days and non- $O_3$ -exceeding days. The increase in  $O_3$ -exceeding days is the primary contributor to the substantial increase in the annual mean  $O_3$  in all three megacity clusters  
115 from 2015 to 2020. The contribution of  $O_3$ -exceeding days is affected mostly by the changing number of exceeding days (more than 80%), and secondly but nevertheless significantly by their changes in concentrations (less than 20%) (Tables 2–4). e.g., in BTH the exceeding days were 31, 43, 62, 74, 96 and 78 days in the individual years of 2015–2020, respectively, while their concentrations of those years were 66.42, 64.13, 69.44, 68.21, 70.19 and 69.69, respectively (Table 2 second column). Contributions from non- $O_3$ -exceeding days are insignificant ( $p > 0.1$ ), except that in BTH (Fig. 2a) which shows a significant  
120 declining contribution ( $p = 0.02$ ) due to the reduced number of non- $O_3$ -exceeding days. Therefore, the following discussions on the  $O_3$  trends will be focused on the  $O_3$ -exceeding days.

Annual numbers of single and consecutive  $O_3$ -exceeding days are shown in Figs. 3a, 3b and 3c for BTH, YRD and PRD, respectively. A drastic two to three-fold increase in the annual numbers of consecutive  $O_3$ -exceeding days can be seen in all three regions. In contrast, the numbers of single  $O_3$ -exceeding days show only a slight increase in PRD. These drastic increases  
125 in the annual numbers of consecutive  $O_3$ -exceeding days are clearly the primary contributors to the trends in  $O_3$  shown in Figs.



2a, 2b and 2c. This brings up several key scientific questions: What is the cause(s) of the drastic increases in the numbers of consecutive O<sub>3</sub>-exceeding days? Is it due to changing O<sub>3</sub> photochemical processes or changing meteorological parameters?

### 3.2 Spatial expansion and quasi-saturation of high O<sub>3</sub>

Another important changing characteristics of O<sub>3</sub> concentrations is illustrated in Fig. 4a, which depicts the annual mean concentrations of MDA8 O<sub>3</sub> in BTH during O<sub>3</sub>-exceeding days for all 78 stations (black line), 14 stations in the highest category of O<sub>3</sub> concentration (average 103 ppb) observed in 2015 (red line, denoted high O<sub>3</sub> stations hereafter, Table 1) and 13 stations in the lowest category of O<sub>3</sub> (average 57 ppb) observed in 2015 (green line, denoted low O<sub>3</sub> stations hereafter, Table 1). It is remarkable that O<sub>3</sub> concentrations at the low O<sub>3</sub> stations caught up within 12 ppb with other stations in merely two years (an increase of about 30 ppb from 2015 to 2017), and actually equaled the average of other stations in 2019. Meanwhile, the high O<sub>3</sub> stations experienced a slight decrease in O<sub>3</sub> concentration, albeit not statistically significant. This phenomenon suggests strongly that the annual mean concentrations of MDA8 O<sub>3</sub> in BTH experienced a fast (within two years) and widespread spatial expansion of high O<sub>3</sub> from urban centers to surrounding regions where O<sub>3</sub> concentrations were low in 2015. Temporally most of the expansion was accomplished during 2015–2017. This phenomenon of a fast and widespread expansion of high O<sub>3</sub> concentrations from urban centers to surrounding regions were also observed at a slightly less degree in YRD (Fig. 4b) and PRD (Fig. 4c).

It is worth noting that O<sub>3</sub> concentrations at the high O<sub>3</sub> stations of approximate 100 ppb in 2015 remained nearly constant or slightly declined throughout the entire period of 2015–2020, while the low O<sub>3</sub> stations with O<sub>3</sub> concentrations less than about 75 ppb in 2015 in all three megacity clusters experienced significant enhancements in O<sub>3</sub> concentration (>5 ppb yr<sup>-1</sup>) during 2015–2017 (Figs. 4a, 4b and 4c). This near-constant O<sub>3</sub> phenomenon suggests a quasi-saturation effect of O<sub>3</sub> formation when the annual mean concentration of MDA8 O<sub>3</sub> reached approximately 100 ppb.

The expansion and quasi-saturation of O<sub>3</sub> raises some interesting scientific questions: What is the cause(s) of the expansion and quasi-saturation? Why did the expansion and quasi-saturation happen mostly during 2015–2017? Did it have anything to do with the increase of consecutive O<sub>3</sub>-exceeding days as suggested in Fig. 3? These questions are addressed in the following section by examining in detail the spatial expansion of high O<sub>3</sub> from urban centers to surrounding regions in BTH, YRD and PRD during 2015–2017.

The spatial expansion of high O<sub>3</sub> from urban centers to surrounding regions in BTH and YRD during 2015–2017 can be clearly visualized in Figs. 5 and 6, respectively. Figures 5a, 5b and 5c show the spatial distribution of daily mean concentrations of MDA8 O<sub>3</sub> for O<sub>3</sub>-exceeding days in BTH in 2015, 2017 and their difference (2017 minus 2015), respectively. Comparing Fig. 5a to 5b, one can see that the area inside the 80-ppb contour (75 ppb is the O<sub>3</sub> exceeding standard) expanded by about a factor of five from 2015 to 2017. The daily average concentration of MDA8 O<sub>3</sub> within the BTH box increased from 66.42 ppb in 2015 (31 days, Fig. 5a) to 69.44 in 2017 (62 days, Fig. 5b), which was a difference of 3.02 ppb or a merely 4.5% increase between the two years (Fig. 5c). When accounted for the number of O<sub>3</sub>-exceeding days, the ratio of MDA8 O<sub>3</sub> in all O<sub>3</sub>-exceeding days between 2017 and 2015 became 2.09. The calculation formula is:



$$(69.44 \times 62) / (66.42 \times 31) = 2.09$$

160 This implied that the increase in  $O_3$  in BTH between 2015 and 2017 shown in Fig. 2a (red line) was almost entirely (95.5%)  
due to the increase in the number of  $O_3$ -exceeding days. These results together with those shown in Fig. 3a suggest that the  
increase in  $O_3$  in BTH between 2015 and 2017 was driven primarily by the increase of consecutive  $O_3$ -exceeding days. Spatially  
Fig. 5c shows the expansion is mostly to the south and southwest outside of BTH, with YRD getting a lion's share of  $O_3$   
enhancements. Within the BTH box, the nearly constant concentrations of  $O_3$  inside Beijing City ( $40^\circ N$ ,  $116.5^\circ E$ ) coupled  
165 with the southwestward expansion of high  $O_3$  in 2017 (Fig. 5c) suggested that there was a quasi-saturation of  $O_3$  inside Beijing  
City, and an expansion of weather systems conducive to  $O_3$  formation from Beijing toward the southwest of the BTH box  
during 2017 (Figs. 5b and 5c). This change of weather conditions also caused significant increases in  $O_3$  in YRD and even in  
southern China as far as the western PRD (Fig. 5c). Nevertheless, the  $O_3$  concentrations in YRD and PRD stayed below 70  
ppb during the  $O_3$ -exceeding days of BTH in both 2015 (Fig. 5a) and 2017 (Fig. 5b). In other words, the  $O_3$ -exceeding days of  
170 YRD and PRD are mostly decoupled (i.e., not occurring at the same time) from those of BTH. A logical explanation for this  
phenomenon is that the atmospheric conditions conducive to high  $O_3$  formation in BTH do not overlap significantly with those  
conditions of YRD and PRD.

Figs. 6a, 6b and 6c are the same as Figs. 5a, 5b and 5c, respectively, except for YRD. Similar to BTH, one can clearly see the  
expansion of high  $O_3$  from the vicinity of Shanghai City ( $31^\circ N$ ,  $121.3^\circ E$ ) in the northwestern direction reaching as far as the  
175 central BTH box during the period 2015–2017 (Figs. 6b and 6c). Comparing Fig. 6a to 6b, one can see that the area inside the  
70-ppb contour expanded from Shanghai and vicinity northwestward by more than a factor of five from 2015 to 2017. This  
expansion was in different direction from the southwestern expansion occurred in BTH (Fig. 5c). Since it is highly unlikely  
that any change in emissions could result in these different expansions in YRD and BTH, the logical explanation of the  
expansion in YRD would be that the weather system conducive to  $O_3$  formation moved from the vicinity of Shanghai in 2015  
180 (Fig. 6a) northwestward toward western BTH in 2017 (Figs. 6b and 6c). We note, however, this movement of the weather  
system does not necessarily mean the direct transport of high  $O_3$  or its precursors from the vicinity of Shanghai to central BTH.  
In fact, the presence of separate rather than contiguous red patches of high  $O_3$  ( $>70$  ppb) in southern BTH and northern YRD  
in Fig. 6b is a clear indication that the high  $O_3$  are primarily controlled by local photochemical production from local  $O_3$   
precursors under the expanded conducive weather conditions, rather than the direct upwind-downwind transport of high  $O_3$  or  
185 its precursors. The daily average MDA8  $O_3$  in the YRD box increased from 53.79 ppb in 2015 (31 days, Fig. 6a) to 64.35 in  
2017 (40 days, Fig. 6b), which was a difference of 10.56 ppb or a 20% increase between the two years (Fig. 6c). When  
accounted for the number of  $O_3$ -exceeding days, the ratio of MDA8  $O_3$  in all  $O_3$ -exceeding days between 2017 and 2015  
became:

$$(64.35 \times 40) / (53.79 \times 31) = 1.54 (+54\%)$$

190 This implied that the increase in  $O_3$  in YRD between 2015 and 2017 shown in Fig. 2b (red line) was due to both the increases  
in  $O_3$  concentrations (+20%) and the number of  $O_3$ -exceeding days (+34%).





Figs. 7a, 7b and 7c are the same as Figs. 5a, 5b and 5c, respectively, except they are for PRD. Unlike BTH and YRD, there was only a slight expansion of high O<sub>3</sub> within the PRD box toward the southwest in 2017 compared to 2015 (Fig. 7c). Nevertheless, outside the PRD box there was an extensive expansion of high O<sub>3</sub> in eastern China, substantially greater than the expansion within the PRD box (Fig. 7c). The daily average concentration of MDA8 O<sub>3</sub> within the PRD box increased from 61.16 ppb in 2015 (14 days, Fig. 7a) to 65.18 in 2017 (36 days, Fig. 7b), which was a difference of 4.02 ppb or a merely 6.6% increase between the two years (Fig. 7c). After accounting for the number of O<sub>3</sub>-exceeding days, the ratio of MDA8 O<sub>3</sub> in all O<sub>3</sub>-exceeding days between 2017 and 2015 became 2.74. The calculation formula is:

$$(65.18 \times 36) / (61.16 \times 14) = 2.74$$

This implied that the increase in O<sub>3</sub> in PRD between 2015 and 2017 shown in Fig. 2c (red line) was almost entirely (93.4%) due to the increase in the number of O<sub>3</sub>-exceeding days.

Figures 7a and 7b reconfirm that O<sub>3</sub>-exceeding days in PRD were mostly decoupled from those in BTH (Figs. 5a and 5b) and YRD (Figs. 6a and 6b), as their spatial distributions were characterized by highly distinctive regional features in both 2015 and 2017. These differences suggest that the O<sub>3</sub>-exceeding days mostly occur in different days in the three individual regions. On the other hand, a comparison of Figs. 7c, 6c and 5c reveals a striking common feature of high values in southwestern BTH and northwestern YRD, and low values in eastern parts of all three BTH, YRD and PRD boxes. These common features suggest that the difference between 2015 and 2017 in all three individual regions is likely caused by a common mechanism/process that changed from 2015 to 2017. Moreover, as suggested in Fig. 3, this common mechanism/process must be closely related to higher number of consecutive O<sub>3</sub>-exceeding days in 2017 over those of 2015.

More evidence against the emissions of air pollutants as a major cause of the expansion and quasi-saturation can be seen in Fig. 8, in which the annual mean concentrations of MDA8 O<sub>3</sub> during O<sub>3</sub>-exceeding days are compared to those of O<sub>x</sub> (O<sub>3</sub>+NO<sub>2</sub>) as well as other air pollutants in BTH in 2015–2020. The nearly 30 ppb increases in O<sub>3</sub> (Fig. 8a) at low O<sub>3</sub> stations from 2015 to 2017 occurred also in O<sub>x</sub> (Fig. 8b), suggesting that titration by NO or emission of NO was not the cause of the increases in O<sub>3</sub> in 2015–2017, even though the titration effect may well be the cause of the smaller overall trend in O<sub>3</sub> during much longer period 2006–2019 as suggested convincingly by Li et al. (2022). In addition, PM<sub>2.5</sub> concentrations at high O<sub>3</sub> stations in Fig. 8c decreased significantly more than those at low O<sub>3</sub> stations from 2015 to 2017, yet the low O<sub>3</sub> stations experienced a near 30 ppb increase in O<sub>3</sub>, while O<sub>3</sub> remained essentially constant at the high O<sub>3</sub> stations, suggesting that the proposed removal of HO<sub>2</sub> radicals by PM<sub>2.5</sub> (Li K. et al., 2021; Shao et al., 2021) was also not a likely cause of the increases in O<sub>3</sub> in 2015–2017. In this context, it should be pointed out that we do not doubt the validity of HO<sub>2</sub> removal by PM<sub>2.5</sub>, but its effect was obviously too small to impact on the O<sub>3</sub> trend in 2015–2017. Finally, neither CO nor NO<sub>2</sub> showed any notable change at low O<sub>3</sub> stations between 2015 and 2017, implying negligible change in O<sub>3</sub> precursors, NO<sub>x</sub> and VOCs, as their emission rates tended to be proportional to those of NO<sub>2</sub> and CO, respectively. This again supported the notion that changes in the emissions of O<sub>3</sub> precursors were unlikely to be the driving cause of the increases in O<sub>3</sub> at low O<sub>3</sub> stations from 2015 to 2017.

Comparison of Figure 8a to Figure 1 reveals an interesting point: While the yearly average MDA8 O<sub>3</sub> concentrations at all stations in BTH (green line in Figure 1) shows a significant positive O<sub>3</sub> trend of 2.38 ppb yr<sup>-1</sup> with p=0.01, the black line in



Fig. 8a (MDA8 O<sub>3</sub> of all stations during O<sub>3</sub> exceeding days) shows an insignificant increasing trend of 1.22 ppb yr<sup>-1</sup> with p=0.2. This is because the values in Fig. 8 are those of O<sub>3</sub> exceeding days, of which O<sub>3</sub> concentrations at high O<sub>3</sub> stations (red line in Fig. 8a) have a small decreasing trend (albeit insignificant) due to the quasi-saturation effect discussed above. This decreasing trend is the main contributor to the high p value of 0.2 of the black line in Fig. 8a (all stations).

### 230 3.3 Cause(s) of the expansion and quasi-saturation

Major findings of subsections 3.1 and 3.2 can be summarized as follows: (1) Trends in O<sub>3</sub> observed in the three megacity clusters in eastern China during 2015–2020 (Fig. 1) were mainly caused by the large trends of approximately two to three-fold increase in the number of consecutive O<sub>3</sub>-exceeding days (Figs. 2 and 3). (2) A fast and widespread expansion of high O<sub>3</sub> from urban centers to surrounding regions was observed in the three megacity clusters during 2015–2019 (Fig. 4); and the majority  
235 of the expansions were accomplished during the 2015–2017 period (green lines in Fig. 4). (3) The expansions of high O<sub>3</sub> in the three megacity clusters were accompanied by a quasi-saturation effect that O<sub>3</sub> concentrations at the high O<sub>3</sub> stations (high O<sub>3</sub> in 2015) of approximate 100 ppb in 2015 remained nearly constant throughout the entire period of 2015–2020, while the low O<sub>3</sub> stations (low O<sub>3</sub> in 2015) with O<sub>3</sub> of about 75 ppb in all three megacity clusters in 2015 experienced significant  
240 enhancements in O<sub>3</sub> (>5 ppb yr<sup>-1</sup>) during 2015–2017 (Figs. 4a, 4b and 4c). And (4) There is independent evidence, including spatial distribution of the expansion (Figs. 5 and 6) and inter-annual variations in O<sub>3</sub>, O<sub>x</sub>, NO<sub>2</sub>, CO and PM<sub>2.5</sub> (Fig. 8), suggesting that transport/meteorology rather than emissions of O<sub>3</sub> precursors would more likely be the major cause of the expansion and quasi-saturation. In the following, we explore the evidence in support of changing meteorological parameters as a cause of O<sub>3</sub> trends in 2015–2020.

#### 3.3.1 Changes in meteorological parameters as a cause of O<sub>3</sub> trends in 2015–2020

245 While a specific process/mechanism has yet to be found as the primary contributor to the trends in O<sub>3</sub> observed in the three megacity clusters, the findings summarized above suggest that an examination into transport/meteorological processes involved in O<sub>3</sub> episodes with consecutive O<sub>3</sub>-exceeding days could provide useful information on the identity of the primary contributor. Using BTH as an example, we address this issue in the following by dividing O<sub>3</sub> episodes of a given year into two groups: the first group has four or more consecutive O<sub>3</sub>-exceeding days (labeled O<sub>3</sub> days<sub>≥4</sub>), the second group has less than  
250 four consecutive O<sub>3</sub>-exceeding days (labeled O<sub>3</sub> days<sub><4</sub>). Figure 9a shows the mean daily O<sub>3</sub> concentrations of the first group in 2015 (mean concentration of 71.14 ppb inside the BTH box, 7 days), Figure 9b shows the mean daily O<sub>3</sub> concentrations of the second group (65.04 ppb, 24 days), and Fig. 9c is the difference between the two groups (6.10 ppb, Table 2). Figures 9d–9f are the same as Figs. 9a–9c, respectively, except for 2017. The first group in 2017 had 28 days and mean O<sub>3</sub> of 74.43 ppb inside the BTH box, while the second group had 34 days and 65.32 ppb (Table 2). One of the most remarkable differences  
255 between 2017 and 2015 in Figs. 9a–9f was the large number of days with four or more consecutive O<sub>3</sub>-exceeding days (first group) in 2017 (28 days, Fig. 9d) over that of 2015 (7 days, Fig. 9a), which alone contributed to about 62% of the difference in O<sub>3</sub> between 2017 and 2015 as shown in Fig. 2a (red line). Approximately 30% was contributed by the 10 days' difference





(2017 vs. 2015) in the number of days with less than four consecutive O<sub>3</sub>-exceeding days (second group). The contribution by the higher average concentration of MDA8 O<sub>3</sub> of the first group in 2017 is only about 8% (Table 2). These values of contributions reconfirm what is shown in Fig. 3a, i.e., the greater frequency of episodes with four or more consecutive O<sub>3</sub>-exceeding days contributes the majority (62%) to the higher O<sub>3</sub> in BTH in 2017 vs. 2015, the greater intensity/concentration of O<sub>3</sub> during the episodes contributes only about 8%, consistent with the expansion and quasi-saturation effect discussed earlier. The phenomenon of frequency over intensity is even more pronounced when the data of 2015 (4<sup>th</sup> row and 4<sup>th</sup> column in Table 2) are compared to those of 2019 (8<sup>th</sup> row and 4<sup>th</sup> column in Table 2), in which the higher frequency of the first group of 2019 contributes as much as 83% to the higher O<sub>3</sub> in BTH in 2019 vs. 2015.

The phenomena illustrated in Figs. 9a–9f also exist in YRD and PRD as well as in most other years. Figures equivalent to Figs. 9a–9c for all years in the three city clusters (except PRD during 2015–2016, in which no episode with four or more consecutive O<sub>3</sub>-exceeding days occurred) are provided in the Supplementary Material (Figs. S3–S5). Essential information derived from those figures is summarized in Tables 2–4. The 4<sup>th</sup> column of Table 2 shows that the number of days with four or more consecutive O<sub>3</sub>-exceeding days in BTH increased consistently from 7 days in 2015 to 66 days 2019 and dropped back to 38 days in 2020; this pattern of changes matched very well with those in Fig. 2a (red line). The same can be said for YRD (Table 3) and PRD (Table 4), except there are some minor contributions from the third column in Tables 3 and 4, i.e., days with less than four consecutive O<sub>3</sub>-exceeding days. Another remarkable point is that the difference between ( $\geq 4$ days) and ( $< 4$ days) (5<sup>th</sup> column) in Tables 2–4 is slightly positive (mostly by a few percent) for all three city clusters in all years, which again implies expansion and quasi-saturation of high O<sub>3</sub> in episodes with four or more consecutive O<sub>3</sub>-exceeding days. In summary, Tables 2–4 show quantitatively that the temporal and spatial changes in O<sub>3</sub> concentrations in three megacity clusters of eastern China during 2015–2020 can be mostly attributed to the changes in the number of days with four or more consecutive O<sub>3</sub>-exceeding days. It follows then that the critical question of our quest for the cause(s) of the remarkable large upward linear trend in O<sub>3</sub> of the three megacity clusters becomes: what process/mechanism is conducive to the formation of O<sub>3</sub> episodes with four or more consecutive O<sub>3</sub>-exceeding days?

In Figs. 10a and 10b the values of SSR and T2m of the episodes with four or more consecutive O<sub>3</sub>-exceeding days are compared to those of O<sub>3</sub> episodes with less than four consecutive O<sub>3</sub>-exceeding days, and to those of clean days (non-O<sub>3</sub>-exceeding days). As expected, the O<sub>3</sub> episodes with four or more consecutive O<sub>3</sub>-exceeding days consistently have the highest values of SSR and T2m, while the clean days have the lowest values. This is the case in nearly all years studied as shown in the Supplementary Material (Fig. S6) and is also generally true in YRD and PRD (Figs. S7 and S8). Coupling the higher values of SSR and T2m in the O<sub>3</sub> episodes with four or more consecutive O<sub>3</sub>-exceeding days depicted in Fig. 10 and greater number of days in the O<sub>3</sub> episodes with four or more consecutive O<sub>3</sub>-exceeding days shown in Fig. 3, we therefore propose a hypothesis as follows: the cause of worsening O<sub>3</sub> trends in BTH, YRD and PRD from 2015 to 2020 could be attributed to enhanced photochemical O<sub>3</sub> production due to the increased occurrence of meteorological conditions of high solar radiation and positive temperature anomaly at the surface.



Quantitatively the coupling of Fig. 10 with Fig. 3 can be performed by multiplying the difference between the red (four or more consecutive O<sub>3</sub>-exceeding days) and green (clean days) values of SSR/T2m in Fig. 10 with the frequency of occurrence (in percentage of total days) of O<sub>3</sub> episodes with four or more consecutive O<sub>3</sub>-exceeding days from Fig. 3. The results are compared to the yearly total O<sub>3</sub>-exceeding days in Fig. 11. Correlation between the yearly O<sub>3</sub>-exceeding days and weighed  
295 SSR is very good with R values 0.88 or greater in all three regions, lending strong support for our hypothesis. Correlation between the yearly O<sub>3</sub>-exceeding days and weighed T2m is high correlated in BTH but not correlated in YRD and PRD, which probably suggests that T2m is not as strongly coupled to O<sub>3</sub> formation as SSR. Inclusion of O<sub>3</sub> episodes with less than four consecutive O<sub>3</sub>-exceeding days in Fig. 11 did not change the correction coefficients significantly, supporting the robustness of results shown in Fig.11.

300 The presence of TCs in the northwest Pacific, specific positions and strengths of WPSH in different regions, and mid-high latitude wave activities can contribute to the increased frequency of meteorological conditions characterized by high solar radiation and positive temperature anomalies at the surface (Hu W. et al., 2023; Mao et al., 2020; Ouyang et al., 2022). The contributions of TCs and WPSH are discussed in the following two sections.

### 3.3.2 Contribution of tropical cyclones in PRD

305 In collaboration with this study, Hu W. et al. (2023) conducted a statistical analysis to assess the processes that contribute to high O<sub>3</sub> formation in PRD when TCs occur in the northwest Pacific. They investigated the impact of the distance between TCs in the northwest Pacific and PRD on the O<sub>3</sub> concentration in the PRD from 2006 to 2020. Their findings revealed that the most common process leading to consecutive O<sub>3</sub>-exceeding days, which are responsible for elevated O<sub>3</sub> concentrations, was associated with downdraft and stable atmospheric conditions. These conditions were most frequently observed when TCs were  
310 located in the mid-distance category (700 km–4000 km) from PRD. Interestingly, TCs in this mid-distance category, occurring 49% of the time during the warm season (June–November), accounted for a substantial 80.7% of consecutive O<sub>3</sub>-exceeding days, which was four times higher than the combined consecutive O<sub>3</sub>-exceeding days from the other three categories. As shown in Fig. 3 and Section 3.1 that the interannual variations and trends in the annual mean O<sub>3</sub> concentrations in PRD between 2015 and 2020 were primarily influenced by the occurrence of consecutive O<sub>3</sub>-exceeding days. Consequently, it can be inferred that  
315 TCs in the mid-distance category played a critical role in shaping the interannual variations and trends of O<sub>3</sub> in PRD during the same time period. Quantitatively, Hu W. et al. (2023) found that the downdrafts associated with mid-distance category TCs accounted for 35 consecutive O<sub>3</sub>-exceeding days in 2019, compared to only 10–25 days in other years. Interestingly, the large number of consecutive O<sub>3</sub>-exceeding days in 2019 was primarily attributed to the increased occurrence of downdrafts and stable atmospheric conditions brought about by mid-distance category TCs, rather than the number of TCs, which only showed  
320 a slight increase compared to other years. These results imply that the heightened frequency of downdrafts and stable atmospheric conditions associated with mid-distance category TCs could be the main driver behind the elevated number of consecutive O<sub>3</sub>-exceeding days in 2019, contributing to approximately 80% of the overall trend in O<sub>3</sub> concentrations between 2015 and 2020 (Fig. 3c and black line, Fig.4c). In summary of Section 3.3.1, the mid-distance category TCs could contribute



to about 80% of the overall trend of O<sub>3</sub> in PRD in 2015–2020. Less contributions of TCs to the O<sub>3</sub> trends in YRD and BTH  
325 are expected because of stronger influence of prevailing westerlies at higher latitudes. Nevertheless, similar evaluations for  
these regions would be highly valuable.

### 3.3.3 Contribution of WPSH

Mao et al. (2020) made a comprehensive study of an 11-day O<sub>3</sub> episode in BTH in 2017 and found it was dominated by the  
presence of the WPSH and mid-high latitude wave activities. Depending on the position and intensity, WPSH is well known  
330 to be a crucial factor affecting O<sub>3</sub> concentrations in various parts of eastern China (Chang et al., 2019; Yin et al., 2019; Zhao  
and Wang, 2017). During this 11-day O<sub>3</sub> episode, the ridge line of WPSH maintained at approximately 22°N from June 24 to  
June 29, which in combination with mid-high latitude wave activities induced meteorological conditions highly conducive to  
the O<sub>3</sub> production in BTH and northern YRD (Mao et al., 2020).

Following the analysis of Mao et al. (2020), the impact of WPSH on O<sub>3</sub> in BTH in April–September has been analyzed in Fig.  
335 12 which depicts the composite 500 hPa geopotential height contours, humidity and winds in BTH in April–September for O<sub>3</sub>-  
exceeding days in 2015 (a), clean days in 2015 (b), O<sub>3</sub>-exceeding days in 2017 (c), clean days in 2017 (d), O<sub>3</sub>-exceeding days  
in 2019 (e) and clean days in 2019 (f). The three years 2015, 2017 and 2019 are chosen because their differences in O<sub>3</sub>  
contribute predominately to the overall O<sub>3</sub> trends (Figs. 1–2). The importance of WPSH is clearly visible in all Figs. 12a–12f  
when the 5880 and 5900 gpm isolines (green lines) of O<sub>3</sub>-exceeding days are compared to those of clean days. In all three  
340 years, the WPSH of the former (O<sub>3</sub>-exceeding days) were significantly stronger than the latter (clean days) as evident by the  
strong anticyclonic winds and/or the larger areas inside the 5880 gpm isolines. Even in the case of 2017 when the area inside  
5880 gpm isolines of the former looked to be similar to that of the latter, the appearance of 5900 line in the former indicated a  
stronger WPSH. The strong anticyclonic winds in the former (Figs. 12a, 12c and 12e) force moist air of South China Sea  
northward into southern China and contributed to extensive clouds and precipitation and thus low O<sub>3</sub> formation over southern  
345 China and southern YRD. This difference in the O<sub>3</sub> formation between BTH and southern China provides a good explanation  
to why the O<sub>3</sub>-exceeding days mostly occur in different time periods in the three megacity clusters as discussed in Section 3.2.  
Furthermore, over East China Sea the prevailing westerlies were forced northward, slowed down and lead to meteorological  
conditions in BTH and northern YRD characterized by cloudless sky, sinking motion and high vertical stability in the lower  
troposphere, as well as high SSR and positive T2m anomaly at the surface. These meteorological conditions were highly  
350 conducive to the formation and accumulation of O<sub>3</sub>. In contrast, the weaker WPSH of the latter allowed relatively strong  
westerlies to prevail over BTH during clean days in the three years, which tended to disperse O<sub>3</sub> (Figs. 12b, 12d and 12f). e.g.,  
the average wind speed over BTH was about 10 m s<sup>-1</sup> in Fig. 12b, while only about 5 m s<sup>-1</sup> in Fig. 12a. Quantitatively Fig. 12c  
had 31 more O<sub>3</sub>-exceeding days (93 ppb) than Fig. 12a, the 31 days came at the expense of clean days (52 ppb) (Figs. 12b and  
12d). The contribution of these 31 days to the difference in MDA8 O<sub>3</sub> between 2017 and 2015 (6.5 ppb, Fig. 1) can be  
355 calculated as follows:

$$((93 \times 62) + (56 \times 121)) / (62 + 121) - ((86 \times 31) + (52 \times 152)) / (31 + 152) = 10.8 \text{ ppb}$$



This difference of 10.8 ppb in MDA8 O<sub>3</sub> between 2017 and 2015 was for the period of April to September. It should be divided by 2 and became 5.4 ppb for the yearly difference in MDA8 O<sub>3</sub> between 2017 and 2015. This value of 5.4 ppb accounted for 83% of the observed difference in MDA8 O<sub>3</sub> between 2017 and 2015 (6.5 ppb, Fig. 1). Similar statement can be made for the difference in MDA8 O<sub>3</sub> between 2019 and 2017 (Figs. 12e and 12c, Fig. 1).

We have made the same analysis for other years as well as for YRD and PRD. The results are mostly similar, and thus presented in the Supplementary material (Figs. S9, S10 and S11). Figs. 13a–13d for PRD in 2017 and 2019 are shown because there were interesting anticyclonic circulations over PRD during O<sub>3</sub>-exceeding days in both years (Figs. 13a and 13c). The 2017 anticyclone was a direct product of the WPSH as it resided within the western tip of the 5880 gpm isoline. The 2019 anticyclone was also likely associated with the WPSH as the center of anticyclone resided just beneath the 5860 gpm isoline to the west of PRD. The anticyclonic circulations were accompanied by stable downdrafts, low winds, and cloudless sky conditions (short arrows and blue shades in Figs. 13a and 13c), which were highly conducive to the O<sub>3</sub> formation. Cloudless sky conditions also occurred in YRD and BTH in Figs. 13a and 13c, but the high wind speed prevented the accumulation of O<sub>3</sub>. This difference in O<sub>3</sub> accumulation between PRD and other two regions provide another good explanation to why the O<sub>3</sub>-exceeding days mostly occur in different days in the three megacity clusters as discussed in Section 3.2. Quantitatively Fig. 13c had 27 more O<sub>3</sub>-exceeding days (90 ppb) than Fig. 13a, the 27 days came at the expense of clean days (39 ppb) (Figs. 13b and 13d). The contribution of these 27 days to the difference in MDA8 O<sub>3</sub> in PRD between 2019 and 2017 (6.0 ppb, Fig. 1) can be calculated as follows:

$$((90 \times 62) + (46 \times 182)) / (62 + 182) - ((85 \times 35) + (39 \times 209)) / (35 + 209) = 11.6 \text{ ppb}$$

This difference of 11.6 ppb in MDA8 O<sub>3</sub> between 2019 and 2017 was for the period of April to November. It should be divided by 365/244 and became 7.75 ppb for the yearly difference in MDA8 O<sub>3</sub> between 2019 and 2017. This value of 7.75 ppb was 1.75 ppb more than the observed difference in MDA8 O<sub>3</sub> between 2019 and 2017 (6.3 ppb, Fig. 1), suggesting a reduction of about 3.5 ppb in MDA8 O<sub>3</sub> in the cold months of January–March and December between 2017 and 2019, which was approximately confirmed by the observed reduction of 3.88 ppb.

The presence of anticyclonic circulations over PRD is in good agreement with the results of Ouyang et al. (2022) and Hu W. et al. (2023). The latter authors suggested that the anticyclonic circulations over PRD were primarily caused by TCs in northwestern Pacific. Nevertheless, it is widely acknowledged that the tracks of TCs in the northwestern Pacific are influenced, at least to some extent, by WPSH (Sun et al., 2015; Wang et al., 2017), making it difficult to separate the roles played by the TCs on the anticyclonic circulations and O<sub>3</sub> formation from those of WPSH. Clearly, further investigations is needed to fully understand the complex relationship among WPSH, TCs and O<sub>3</sub>. Based on these results, we hypothesize that the increased frequency of these meteorological conditions enabled by the changing intensity and position of WPSH could contribute as a major cause of the positive O<sub>3</sub> trends in the three megacity clusters in eastern China during 2015–2020.

### 3.4 Uncertainty and cautionary statements

It is worth noting that the analyses conducted in Sections 3.1–3.3 have predominantly relied on correlation or regression analysis techniques, which do not imply a cause-and-effect relationship. To establish a cause-and-effect link between the



proposed changes in meteorological parameters and O<sub>3</sub> trends, it is necessary to employ a mechanistic model that is based on the proposed causes and can accurately reproduce the observed O<sub>3</sub> trend. Until such model reproduction is achieved, all correlation or regression findings should be considered as a potential maximum cause-and-effect relationship (Wu et al., 2022). However, current mechanistic models suffer from significant uncertainties, making it difficult to credibly simulate critical atmospheric processes that regulate O<sub>3</sub> formation. These processes include atmospheric transport parameterizations, the sources and sinks of OH, HO<sub>2</sub> and RO<sub>2</sub> radicals, and the photochemistry of VOCs and OVOCs.

#### 4 Summary and Conclusions

Thanks to a strong emission control policy, major air pollutants in China, including PM<sub>2.5</sub>, SO<sub>2</sub>, NO<sub>2</sub> and CO had shown remarkable reductions during 2015–2020. However, O<sub>3</sub> concentration had increased significantly and emerged as a major air pollutant in eastern China during the same time period. The annual mean concentration of MDA8 in three megacity clusters in eastern China, namely BTH, YRD and PRD, showed alarming large upward linear trends of 25%, 10% and 19%, respectively during 2015–2019. Identifying the causes of these worsening O<sub>3</sub> trends is urgently required for air pollution prevention and management.

Some recent studies suggested that enhanced photochemical processes induced by changing anthropogenic emissions were responsible for these trends (Li et al., 2019; Li et al., 2022; Shao et al., 2021; Wang et al., 2020). However, we noticed that there was independent evidence, including the spatial distribution of the expansion of high O<sub>3</sub> (Figs. 5 and 6) and inter-annual variations in O<sub>3</sub>, Ox, NO<sub>2</sub>, CO and PM<sub>2.5</sub> (Fig. 8), suggesting that transport/meteorological conditions rather than emissions of O<sub>3</sub> precursors were more likely to be the major contributor to the O<sub>3</sub> trends. Moreover, we found that the trends in O<sub>3</sub> observed in the three megacity clusters during 2015–2020 (Fig. 1) were mainly caused by the large trend of approximately two to three-fold increase in the number of consecutive O<sub>3</sub>-exceeding days (Fig. 3), during that time a fast and widespread expansion of high O<sub>3</sub> from urban centers to surrounding regions was observed (Fig. 4), and the majority of the expansions was accomplished during the two-year 2015–2017 period (green lines in Fig. 4). Furthermore, the expansions of high O<sub>3</sub> in the three megacity clusters were accompanied by a quasi-saturation effect that O<sub>3</sub> concentrations at the high O<sub>3</sub> stations (high O<sub>3</sub> in 2015) of approximate 100 ppb remained nearly constant throughout the entire period of 2015–2020, while the low O<sub>3</sub> stations (low O<sub>3</sub> in 2015) with O<sub>3</sub> less than 75 ppb in all three megacity clusters experienced a significant enhancement in O<sub>3</sub> (>5 ppb yr<sup>-1</sup>) during 2015–2017 (Figs. 4a, 4b and 4c). Finally, greater frequency of episodes with four or more consecutive O<sub>3</sub>-exceeding days contributed the majority to the higher O<sub>3</sub> in all three megacity clusters in 2017 vs. 2015, the greater intensity/concentration of O<sub>3</sub> during the episodes contributes only about 10% (Fig. 9), consistent with the expansion and quasi-saturation effect discussed earlier.

Coupling the higher values of SSR and T2m in the O<sub>3</sub> episodes with four or more consecutive O<sub>3</sub>-exceeding days depicted in Fig. 10 and greater occurrence (number of days) in the O<sub>3</sub> episodes with four or more consecutive O<sub>3</sub>-exceeding days shown in Fig. 3, we hypothesize that the cause of the worsening O<sub>3</sub> trends in BTH, YRD and PRD from 2015 to 2020 could be



425 attributed to enhanced photochemical O<sub>3</sub> production due to the increased occurrence of meteorological conditions of high solar radiation and positive temperature anomaly under the influence of WPSH and TCs. The hypothesis is substantiated in Fig. 11, which shows excellent correlation between the yearly O<sub>3</sub>-exceeding days and SSR with R values 0.88 or greater in all three regions. Correlation between the yearly O<sub>3</sub>-exceeding days and T2m is good in BTH but poor in YRD and PRD, which probably suggests that T2m is not as strongly coupled to O<sub>3</sub> formation as SSR.

In conjunction with our study, Hu W. et al. (2023) conducted a statistical analysis to evaluate the processes that promote high O<sub>3</sub> formation in PRD when TCs are present in the northwest Pacific. They assessed the impact of the distance between a TC 430 in the northwest Pacific and PRD on O<sub>3</sub> in the PRD from 2006 to 2020. They found that the increased frequency of the downdrafts and stable atmosphere conditions brought forth by the mid-distance category TCs could be the main cause of the large number of consecutive O<sub>3</sub>-exceeding days in 2019, which contribute to about 80% of the overall positive trend of O<sub>3</sub> in 2015–2020 (Fig. 3c and black line, Fig.4c).

Following the analysis of Mao et al. (2020), the impact of WPSH on O<sub>3</sub> in BTH in April–September has been analyzed in Fig. 435 12. We found that the increased frequency of these meteorological conditions enabled by the changing intensity and position of WPSH could contribute as a major cause of the positive O<sub>3</sub> trends in the three megacity clusters in eastern China during 2015–2020.

Nevertheless, it is crucial to recognize that the examinations carried out in Sections 3.1–3.3 primarily utilized correlation or regression analysis techniques, which do not inherently establish causal relationships. To attribute cause and effect between 440 the suggested alterations in meteorological parameters and O<sub>3</sub> trends, it is necessary to employ a mechanistic model that accurately replicates the observed O<sub>3</sub> trend based on the proposed cause(s). Until the model successfully reproduces the phenomenon, all correlation or regression findings should be treated as merely indicating the highest potential cause-and-effect relationship (Wu et al., 2022).

In conclusion, we hypothesize that the cause of the worsening O<sub>3</sub> trends in BTH, YRD and PRD from 2015 to 2020 is 445 attributable to enhanced photochemical O<sub>3</sub> production due to the increased occurrence of meteorological conditions of high solar radiation and positive temperature anomaly under the influence of WPSH and TCs. Therefore, we suggest that future O<sub>3</sub> pollution prevention and control policies should pay more attention to changes in the meteorological/climate conditions, particularly changes in the large-scale circulations, including WPSH and TCs.

450 *Data availability.* Hourly surface O<sub>3</sub>, NO<sub>2</sub>, CO, PM<sub>2.5</sub>, and SO<sub>2</sub> data were obtained from China National Environmental Centre (<http://www.cnemc.cn/en/>). Hourly meteorological data are obtained from European Centre for Medium-Range Weather Forecasts ERA5 reanalysis (<https://cds.climate.copernicus.eu/>). Daily meteorological data are obtained from National Center for Environmental Prediction (NCEP) and National Center for Atmospheric Research (NCAR) (<https://psl.noaa.gov/data/gridded/data.ncep.reanalysis.html>). The data of this study are available upon request to Shaw Chen 455 Liu ([shawliu@jnu.edu.cn](mailto:shawliu@jnu.edu.cn)).





*Author Contributions.* SL and RL proposed the essential research idea. TH, and YL performed the analysis. TH, YL, RL, and SL drafted the manuscript. YX, BW, and YZ helped analysis and offered valuable comments. All authors have read and agreed to the published version of the manuscript.

460

*Competing interests.* The authors declare that they have no conflict of interest.

*Acknowledgments.* The authors thank the China National Environmental Centre and European Centre for Medium-Range Weather Forecasts for providing datasets that made this work possible. We also acknowledge the support of the Institute for Environmental and Climate Research and Guangdong-Hongkong-Macau Joint Laboratory of Collaborative Innovation for Environmental Quality in Jinan University.

*Financial support.* This research was supported by the National Natural Science Foundation of China (grant number 92044302, 41805115), Guangzhou Municipal Science and Technology Project, China (grant number 202002020065), Special Fund Project for Science and Technology Innovation Strategy of Guangdong Province (grant number 2019B121205004), Guangdong Innovative and Entrepreneurial Research Team Program (grant number 2016ZT06N263), and National Key Research and Development Program of China (grant number 2018YFC0213906).



## References

- 475 Bachmann, J. D.: Air quality and climate connections, *J. Air Waste Manage.*, 65, 641–644, <https://doi.org/10.1080/10962247.2015.1040697>, 2015.
- Bell, M. L., Peng, R. D., and Dominici, F.: The exposure–response curve for ozone and risk of mortality and the adequacy of current ozone regulations, *Environ. Health Perspect.*, 114, 532–536, <https://doi.org/10.1289/ehp.8816>, 2006.
- Bian, Y., Huang, Z., Ou, J., Zhong, Z., Xu, Y., Zhang, Z., Xiao, X., Ye, X., Wu, Y., Yin, X., Li, C., Chen, L., Shao, M., and  
480 Zheng, J.: Evolution of anthropogenic air pollutant emissions in Guangdong Province, China, from 2006 to 2015, *Atmos. Chem. Phys.*, 19, 11701–11719, <https://doi.org/10.5194/acp-19-11701-2019>, 2019.
- Chang, L., Xu, J., Tie, X., and Gao, W.: The impact of Climate Change on the Western Pacific Subtropical High and the related ozone pollution in Shanghai, China, *Sci. Rep.*, 9, 16998, <https://doi.org/10.1038/s41598-019-53103-7>, 2019.
- Chen, Z., Li, R., Chen, D., Zhuang, Y., Gao, B., Yang, L., and Li, M.: Understanding the causal influence of major  
485 meteorological factors on ground ozone concentrations across China, *J. Clean. Prod.*, 242, 118498, <https://doi.org/10.1016/j.jclepro.2019.118498>, 2020.
- Cohen, A. J., Brauer, M., Burnett, R., Anderson, H. R., Frostad, J., Estep, K., Balakrishnan, K., Brunekreef, B., Dandona, L., Dandona, R., Feigin, V., Freedman, G., Hubbell, B., Jobling, A., Kan, H., Knibbs, L., Liu, Y., Martin, R., Morawska, L., Pope III C. A., Shin, H., Straif, K., Shaddick, G., Thomas, M., van Dingenen, R., van Donkelaar, A., Vos, T., Murray, C. J. L., and  
490 Forouzanfar, M. H.: Estimates and 25-year trends of the global burden of disease attributable to ambient air pollution: an analysis of data from the Global Burden of Diseases Study 2015, *The Lancet*, 389, 1907–1918, [https://doi.org/10.1016/S0140-6736\(17\)30505-6](https://doi.org/10.1016/S0140-6736(17)30505-6), 2017.
- Deng, T., Wang, T., Wang, S., Zou, Y., Yin, C., Li, F., Liu, L., Wang, N., Song, L., Wu, C., and Wu, D.: Impact of typhoon periphery on high ozone and high aerosol pollution in the Pearl River Delta region, *Sci. Total Environ.*, 668, 617–630,  
495 <https://doi.org/10.1016/j.scitotenv.2019.02.450>, 2019.
- Dong, Y., Li, J., Guo, J., Jiang, Z., Chu, Y., Chang, L., Yang, Y., and Liao, H.: The impact of synoptic patterns on summertime ozone pollution in the North China Plain, *Sci. Total Environ.*, 735, 139559, <https://doi.org/10.1016/j.scitotenv.2020.139559>, 2020.
- Fu, Y., Liao, H., and Yang, Y.: Interannual and decadal changes in tropospheric ozone in China and the associated chemistry-climate interactions: a review, *Adv. Atmos. Sci.*, 36, 975–993, <https://doi.org/10.1007/s00376-019-8216-9>, 2019.
- 500 Gao, D., Xie, M., Chen, X., Wang, T., Liu, J., Xu, Q., Mu, X., Chen, F., Li, S., Zhuang, B., Li, M., Zhao, M., and Ren, J.: Systematic classification of circulation patterns and integrated analysis of their effects on different ozone pollution levels in the Yangtze River Delta Region, China. *Atmos. Environ.*, 242, 117760, <https://doi.org/10.1016/j.atmosenv.2020.117760>, 2020.
- Guo, H., Chen, K., Wang, P., Hu, J., Ying, Q., Gao, A., and Zhang, H.: Simulation of summer ozone and its sensitivity to  
505 emission changes in China, *Atmos. Pollut. Res.*, 10, 543–1552, <https://doi.org/10.1016/j.apr.2019.05.003>, 2019.



- Han, H., Liu, J., Shu, L., Wang, T., and Yuan, H.: Local and synoptic meteorological influences on daily variability in summertime surface ozone in eastern China, *Atmos. Chem. Physics.*, 20, 203–222. <https://doi.org/10.5194/acp-20-203-2020>, 2020.
- Hu, W., Liu, R., Chen, Z., Ouyang, S., Hu, T., Wang, Y., Cui, Z., Jiang, B., Chen, D., Liu, S.C., Processes conducive to high  
510 ozone formation in Pearl River Delta in the presence of Pacific tropical cyclones, *Atmos. Environ.*, 307, 119859, <https://doi.org/10.1016/j.atmosenv.2023.119859>, 2023.
- Kalabokas, P., Jensen, N.R., Roveri, M., Hjorth, J., Eremenko, M., Cuesta, J., Dufour, G., Foret, G., Beekmann, M.: A study of the influence of tropospheric subsidence on spring and summer surface ozone concentrations at the JRC Ispra station in northern Italy, *Atmos. Chem. Phys.*, 20, 1861–1885, <https://doi.org/10.5194/acp-20-1861-2020>, 2020.
- 515 Lam, Y. F., Cheung, H. M., and Ying, C. C.: Impact of tropical cyclone track change on regional air quality, *Sci. Total Environ.*, 610–611, 1347–1355, <https://doi.org/10.1016/j.scitotenv.2017.08.100>, 2018.
- Li, K., Jacob, D. J., Liao, H., Shen, L., Zhang, Q., and Bates, K. H.: Anthropogenic drivers of 2013–2017 trends in summer surface ozone in China, *Proc. Natl. Acad. Sci. U.S.A.*, 116, 422–427, <https://doi.org/10.1073/pnas.181216811>, 2019.
- Li, K., Jacob, D. J., Liao, H., Qiu, Y., Shen, L., Zhai, S., Bates, K. H., Sulprizio, M. P., Song, S., Lu, X., Zhang, Q., Zheng,  
520 B., Zhang, Y., Lee, H. C., and Su, K. K.: Ozone pollution in the North China Plain spreading into the late-winter haze season, *Natl. Acad. Sci. U.S.A.*, 118, e2015797118, <https://doi.org/10.1073/pnas.2015797118>, 2021.
- Li, M., Wang, T., Shu, L., Qu, Y., Xie, M., Liu, J., Wu, H., Kalsoom, U.: Rising surface ozone in China from 2013 to 2017: A response to the recent atmospheric warming or pollutant controls? *Atmos. Environ.*, 246, 118130, <https://doi.org/10.1016/j.atmosenv.2020.118130>, 2021.
- 525 Li, X., Yuan, B., Parrish, D. D., Chen, D., Song, Y., Yang, S., Liu, Z., Shao, M.: Long-term trend of ozone in southern China reveals future mitigation strategy for air pollution, *Atmos. Environ.*, 269, 118869, <https://doi.org/10.1016/j.atmosenv.2021.118869>, 2022.
- Liu, H., Liu, S., Xue, B., Lv, Z., Meng, Z., Yang, X., Xue, T., Yu, Q., and He, K.: Ground-level ozone pollution and its health impacts in China, *Atmos. Environ.*, 173, 223–230, <https://doi.org/10.1016/j.atmosenv.2017.11.014>, 2018.
- 530 Lu, X., Hong, J., Zhang, L., Cooper, O. R., Schultz, M. G., Xu, X., Wang, T., Gao, M., Zhao, Y., and Zhang, Y.: Severe surface ozone pollution in China: A global perspective, *Environ. Sci. Technol. Lett.*, 5, 487–494, <https://doi.org/10.1021/ACS.ESTLETT.8B00366>, 2018.
- Lu, X., Zhang, L., and Shen, L.: Meteorology and climate influences on tropospheric ozone: a review of natural sources, chemistry, and transport patterns, *Curr. Pollution Rep.*, 5, 238–260, <https://doi.org/10.1007/s40726-019-00118-3>, 2019.
- 535 Ma, J., Xu, X., Zhao, C., and Yan, P.: A review of atmospheric chemistry research in China: Photochemical smog, haze pollution, and gas-aerosol interactions, *Adv. Atmos. Sci.*, 29, 1006–1026, <https://doi.org/10.1007/s00376-012-1188-7>, 2012.
- Mao, J., Wang, L., Lu, C., Liu, J., Li, M., Tang, G., Ji, D., Zhang, N., and Wang, Y.: Meteorological mechanism for a large-scale persistent severe ozone pollution event over eastern China in 2017, *J. Environ. Sci.*, 92, 187–199, <https://doi.org/10.1016/j.jes.2020.02.019>, 2020.



- 540 Monks, P. S., Archibald, A. T., Colette, A., Cooper, O., Coyle, M., Derwent, R., Fowler, D., Granier, C., Law, K. S., Mills, G. E., Stevenson, D. S., Tarasova, O., Thouret, V., von Schneidemesser, E., Sommariva, R., Wild, O., and Williams, M. L.: Tropospheric ozone and its precursors from the urban to the global scale from air quality to short-lived climate forcer, *Atmos. Chem. Phys.*, 15, 8889–8973, <https://doi.org/10.5194/acp-15-8889-2015>, 2015.
- Nuvolone, D., Petri, D., and Voller, F.: The effects of ozone on human health, *Environ. Sci. Pollut. Res. Int.*, 25, 8074–8088, <https://doi.org/10.1007/s11356-017-9239-3>, 2018.
- 545 Ouyang, S., Deng, T., Liu, R., Chen, J., He, G., Leung, J. C.-H., Wang, N., and Liu, S. C.: Impact of a subtropical high and a typhoon on a severe ozone pollution episode in the Pearl River Delta, China, *Atmos. Chem. Phys.*, 22, 10751–10767, <https://doi.org/10.5194/acp-22-10751-2022>, 2022.
- Professional Committee of Ozone Pollution Control of Chinese Society for Environmental Sciences: The Bluebook: Prevention and Control of Ozone Pollution in China (2020), Science Press, Beijing, China, ISBN 978-7-03-071664-4, 2022 (in Chinese).
- 550 Rowlinson, M. J., Rap, A., Arnold, S. R., Pope, R. J., Chipperfield, M. P., McNorton, J., Forster, P., Gordon, H., Pringle, K. J., Feng, W., Kerridge, B. J., Latter, B. L., and Siddans, R.: Impact of El Niño–Southern Oscillation on the interannual variability of methane and tropospheric ozone, *Atmos. Chem. Phys.*, 19, 8669–8686, <https://doi.org/10.5194/acp-19-8669-2019>, 2019.
- 555 Shao, M., Wang, W., Yuan, B., Parrish, D. D., Li, X., Lu, K., Wu, L., Wang, X., Mo, Z., Yang, S., Peng, Y., Kuang, Y., Chen, W., Hu, M., Zeng, L., Su, H., Cheng, Y., Zheng, J., and Zhang, Y.: Quantifying the role of PM<sub>2.5</sub> dropping in variations of ground-level ozone: Inter-comparison between Beijing and Los Angeles, *Sci. Total Environ.*, 788, 147712, <https://doi.org/10.1016/j.scitotenv.2021.147712>, 2021.
- Sun, Y., Zhong, Z., Yi, L., Li, T., Chen, M., Wan, H., Wang, Y., and Zhong, K.: Dependence of the relationship between the tropical cyclone track and western Pacific subtropical high intensity on initial storm size: A numerical investigation. *J. Geophys. Res. Atmos.*, 120(22), 11451–11467, <https://doi.org/10.1002/2015jd023716>, 2015.
- 560 Wang, T., Xue, L., Brimblecombe, P., Lam, Y. F., Li, L., and Zhang, L.: Ozone pollution in China: A review of concentrations, meteorological influences, chemical precursors, and effects, *Sci. Total Environ.*, 575, 1582–1596, <https://doi.org/10.1016/j.scitotenv.2016.10.081>, 2017.
- 565 Wang, Y., Gao, W., Wang, S., Song, T., Gong, Z., Ji, D., Wang, L., Liu, Z., Tang, G., Huo, Y., Tian, S., Li, J., Li, M., Yang, Y., Chu, B., Petäjä, T., Kerminen, V.-M., He, H., Hao, J., Kulmala, M., Wang, Y., and Zhang, Y.: Contrasting trends of PM<sub>2.5</sub> and surface-ozone concentrations in China from 2013 to 2017, *Natl. Sci. Rev.*, 7, 1331–1339, <https://doi.org/10.1093/nsr/nwaa032>, 2020.
- Wei, X., Lam, K.-S., Cao, C., Li, H., and He, J.: Dynamics of the Typhoon Haitang related high ozone episode over Hong Kong, *Adv. Meteorol.*, 6089154, <https://doi.org/10.1155/2016/6089154>, 2016.
- 570 Wu, Y., Liu, R., Li, Y., Dong, J., Huang, Z., Zheng, J., and Liu, S. C.: Contributions of meteorology and anthropogenic emissions to the trends in winter PM<sub>2.5</sub> in eastern China 2013–2018, *Atmos. Chem. Phys.*, 22, 11945–11955, <https://doi.org/10.5194/acp-22-11945-2022>, 2022.



- Xue, T., Zheng, Y., Geng, G., Xiao, Q., Meng, X., Wang, M., Li, X., Wu, N., Zhang, Q., and Zhu, T.: Estimating spatiotemporal variation in ambient ozone exposure during 2013–2017 using a data-fusion model, *Environ. Sci. Technol.*, 54, 14877–14888, <https://doi.org/10.1021/acs.est.0c03098>, 2020.
- Yang, W., Chen, H., Wang, W., Wu, J., Li, J., Wang, Z., Zheng, J., and Chen, D.: Modeling study of ozone source apportionment over the Pearl River Delta in 2015, *Environ. Pollut.*, 253, 393–402, <https://doi.org/10.1016/j.envpol.2019.06.091>, 2019.
- 580 Yang, Y., Liao, H., and Li, J.: Impacts of the East Asian summer monsoon on interannual variations of summertime surface-layer ozone concentrations over China, *Atmos. Chem. Phys.*, 14, 6867–6879, <https://doi.org/10.5194/acp-14-6867-2014>, 2014.
- Yin, Z., Cao, B., and Wang, H.: Dominant patterns of summer ozone pollution in eastern China and associated atmospheric circulations, *Atmos. Chem. Phys.*, 19, 13933–13943, <https://doi.org/10.5194/acp-19-13933-2019>, 2019.
- Zhai, S., Jacob, D. J., Wang, X., Shen, L., Li, K., Zhang, Y., Gui, K., Zhao, T., and Liao, H.: Fine particulate matter (PM<sub>2.5</sub>) trends in China, 2013–2018: separating contributions from anthropogenic emissions and meteorology, *Atmos. Chem. Phys.*, 19, 11031–11041, <https://doi.org/10.5194/acp-19-11031-2019>, 2019.
- 585 Zhang, Y., Tao, M., Zhang, J., Liu, Y., Chen, H., Cai, Z., and Konopka, P.: Long-term variations in ozone levels in the troposphere and lower stratosphere over Beijing: observations and model simulations, *Atmos. Chem. Phys.*, 20, 13343–13354, <https://doi.org/10.5194/acp-20-13343-2020>, 2020.
- 590 Zhang, R.: Relations of water vapor transport from Indian Monsoon with that over East Asia and the summer rainfall in China. *Adv. Atmos. Sci.* 18 (5), 1005–1017, <http://doi.org/10.1007/bf03403519>, 2001.
- Zhao, W., Lü, M., Lu, Q., Gao, B., Liang, X., Liu, M., Sun, J., Chen, L., and Fan, S.: Effects of tropical cyclones on ozone pollution in the Pearl River Delta in autumn, *Environ. Sci.*, 43, 2957–2965, <https://doi.org/10.13227/j.hjcx.202109169>, 2022 (in Chinese).
- 595 Zhao, Z. and Wang, Y.: Influence of the West Pacific subtropical high on surface ozone daily variability in summertime over eastern China, *Atmos. Environ.*, 170, 197–204, <https://doi.org/10.1016/j.atmosenv.2017.09.024>, 2017.
- Zheng, B., Tong, D., Li, M., Liu, F., Hong, C., Geng, G., Li, H., Li, X., Peng, L., Qi, J., Yan, L., Zhang, Y., Zhao, H., Zheng, Y., He, K., and Zhang, Q.: Trends in China's anthropogenic emissions since 2010 as the consequence of clean air actions, *Atmos. Chem. Phys.*, 18, 14095–14111, <https://doi.org/10.5194/acp-18-14095-2018>, 2018.



**Table 1.** Criteria and corresponding numbers of low O<sub>3</sub> and high O<sub>3</sub> stations in the three megacity clusters in 2015. The criterion listed for each megacity cluster was based on the number of MDA8 O<sub>3</sub> exceeding days in 2015. For instance, the criterion for a low O<sub>3</sub> site in BTH was the number of MDA8 O<sub>3</sub> exceeding days in 2015 being less than or equal to 19 days, while for high O<sub>3</sub> site was the number of MDA8 O<sub>3</sub> exceeding days in 2015 being greater than or equal to 71 days.

	Criterion of low O <sub>3</sub> stations	Number of low O <sub>3</sub> stations	Criterion of high O <sub>3</sub> stations	Number of high O <sub>3</sub> stations	Total number of stations
BTH	≤19 days	13	≥ 71 days	14	78
YRD	≤ 37 days	54	≥ 67 days	13	152
PRD	≤ 12days	10	≥46 days	10	48

605





**Table 2.** Mean O<sub>3</sub> concentrations (ppb) and number of days of all O<sub>3</sub>-exceeding days (2nd column), consecutive O<sub>3</sub>-exceeding days with less than four days (3rd column), consecutive O<sub>3</sub>-exceeding days with four or more days (4th column) and the difference between ( $\geq 4$ days) and ( $< 4$ days) (5th column) within the BTH box in 2015–2020.

	All days Concentration (days) ppb	<4 days Concentration (days) ppb	$\geq 4$ days Concentration (days) ppb	Difference ( $\geq 4$ days) – ( $< 4$ days) ppb
2015	66.42(31)	65.04(24)	71.14(07)	6.10
2016	64.13(43)	62.65(26)	66.39(17)	3.74
2017	69.44(62)	65.32(34)	74.43(28)	9.11
2018	68.21(74)	65.43(27)	69.80(47)	4.37
2019	70.19(96)	65.28(30)	72.42(66)	7.14
2020	69.69(78)	65.52(40)	74.08(38)	8.56



610 **Table 3.** Same as Table 2, but for YRD.

	All days Concentration (days) ppb	<4 days Concentration (days) ppb	≥4 days Concentration (days) ppb	Difference (≥4 days) – (<4 days) ppb
2015	53.79(31)	53.59(19)	54.11(12)	0.52
2016	58.87(27)	58.03(23)	63.73(04)	5.70
2017	64.35(40)	62.62(25)	67.22(15)	4.60
2018	63.33(43)	62.49(32)	65.75(11)	3.26
2019	67.18(49)	66.09(27)	68.51(22)	2.42
2020	65.84(38)	64.12(27)	70.06(11)	5.94



**Table 4.** Same as Table 2, but for PRD.

	All days Concentration (days) ppb	<4 days Concentration (days) ppb	≥4 days Concentration (days) ppb	Difference (≥4 days) – (<4 days) ppb
2015	61.16(14)	61.16(14)	---(0)	---
2016	58.44(19)	58.44(19)	---(0)	---
2017	65.18(36)	64.60(23)	66.20(13)	1.60
2018	65.82(31)	63.27(16)	68.55(15)	5.28
2019	69.80(62)	65.96(29)	73.16(33)	7.20
2020	65.08(37)	63.87(22)	66.84(15)	2.97



615

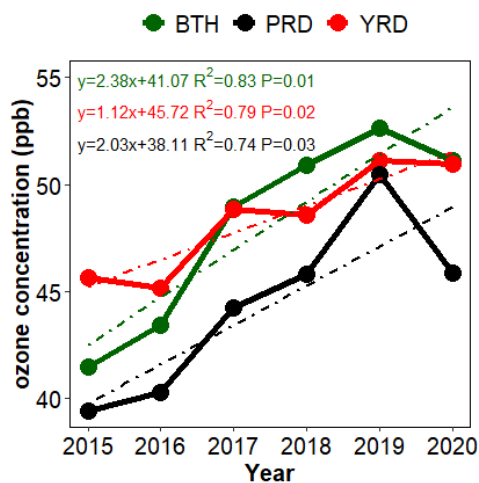
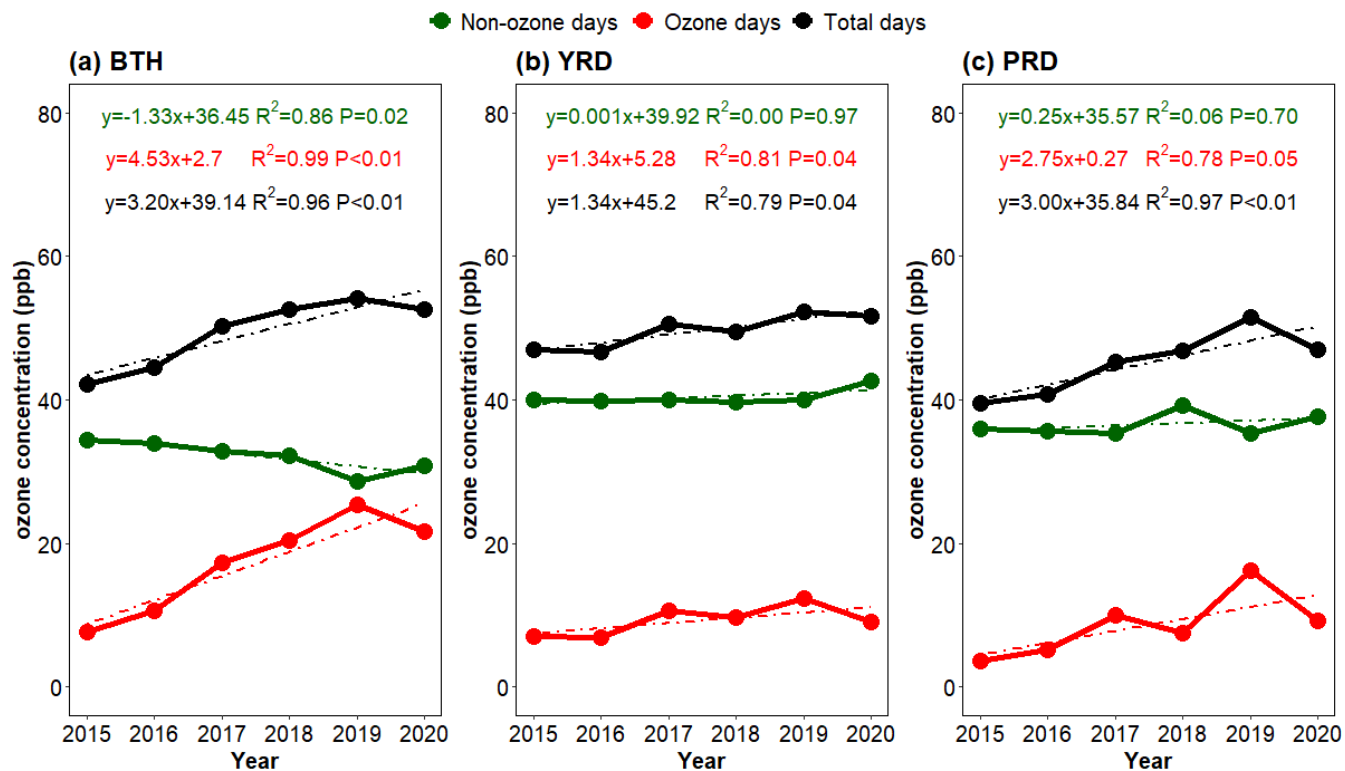
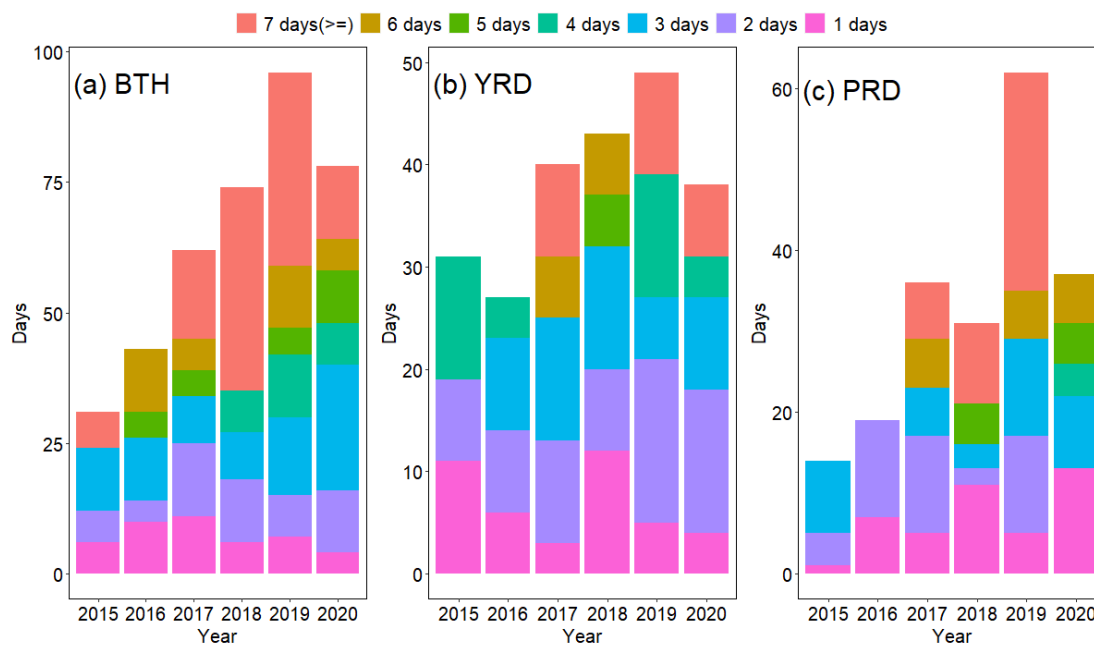


Figure 1: Annual mean concentrations of maximum daily 8-hour average O<sub>3</sub> in BTH (green), YRD (red) and PRD (black).

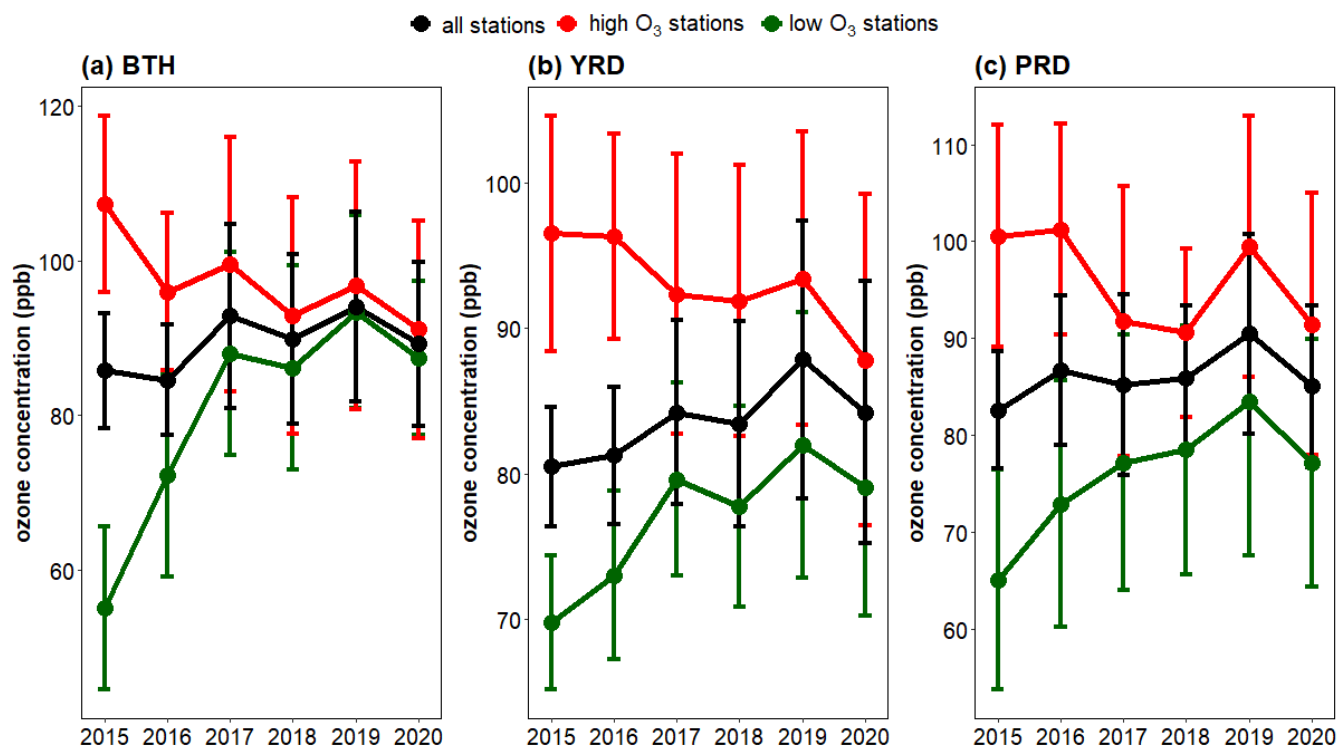


620 **Figure 2: Contributions from the O<sub>3</sub>-exceeding days (red) and non-O<sub>3</sub>-exceeding days (green) to the annual mean concentration of maximum daily 8-hour average O<sub>3</sub> (black) in BTH (a), YRD (b) and PRD (c).**

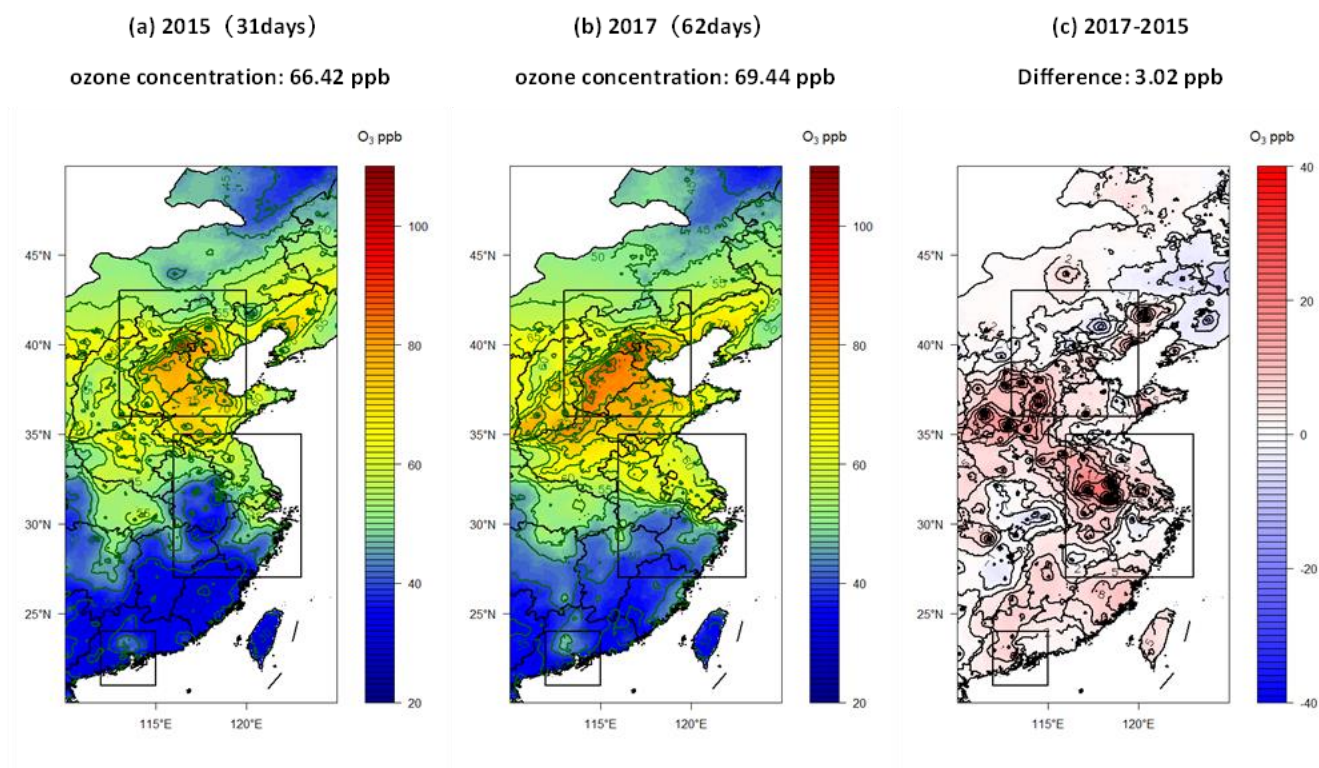


**Figure 3: Annual numbers of various consecutive O<sub>3</sub>-exceeding days in BTH (a), YRD (b) and PRD (c). Individual colors denote different numbers of consecutive O<sub>3</sub>-exceeding days.**





625 Figure 4: Mean concentrations of maximum daily 8-hour average O<sub>3</sub> during O<sub>3</sub>-exceeding days for all stations (black), high O<sub>3</sub> stations (red) and low O<sub>3</sub> stations (green) in BTH (a), YRD (b) and PRD (c).



630 **Figure 5: Spatial distribution of annual mean concentrations of maximum daily 8-hour average O<sub>3</sub> for O<sub>3</sub>-exceeding days in BTH in 2015 (a), 2017 (b) and their difference (2017 - 2015) (c). The top, middle and bottom rectangle boxes denote BTH, YRD and PRD districts, respectively. The number inside the parenthesis behind 2015 or 2017 denotes the number of O<sub>3</sub>-exceeding days.**

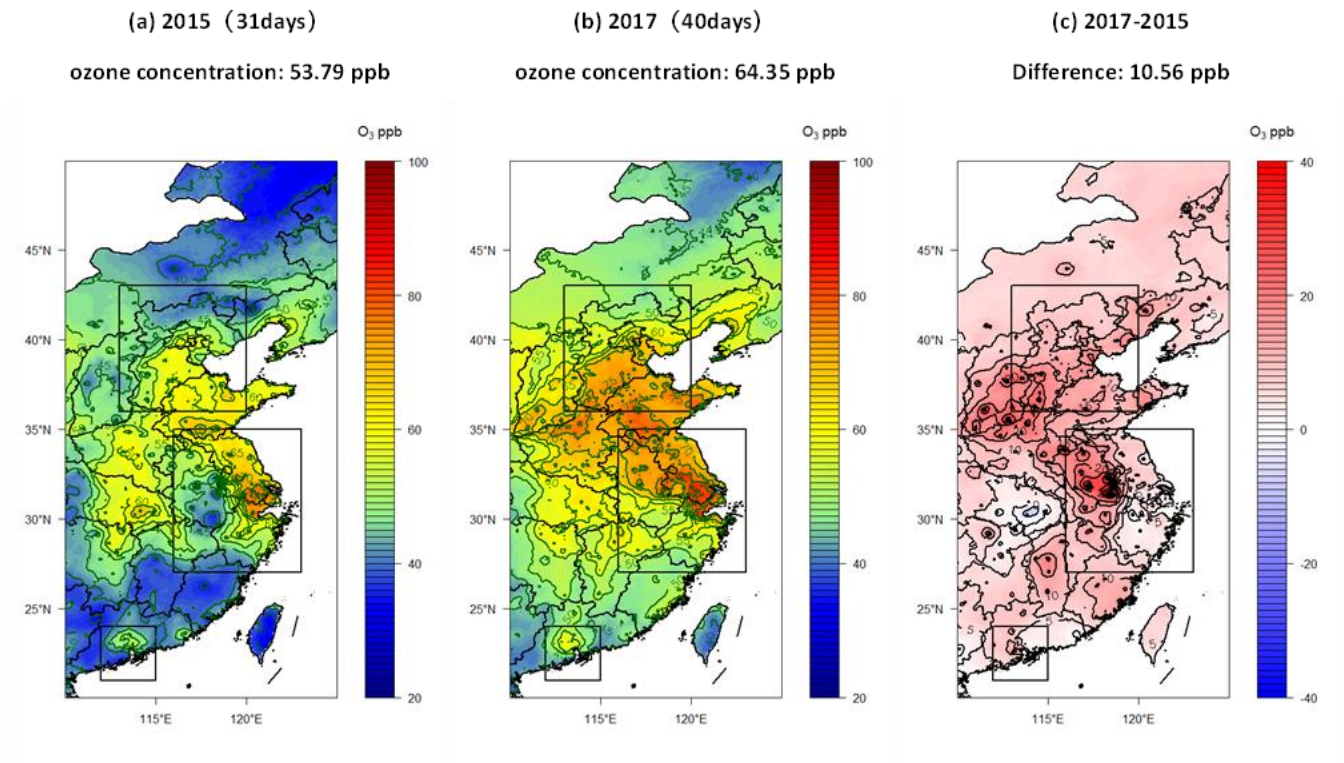


**Figure 6:** Same as Figure 5 except for YRD.



635

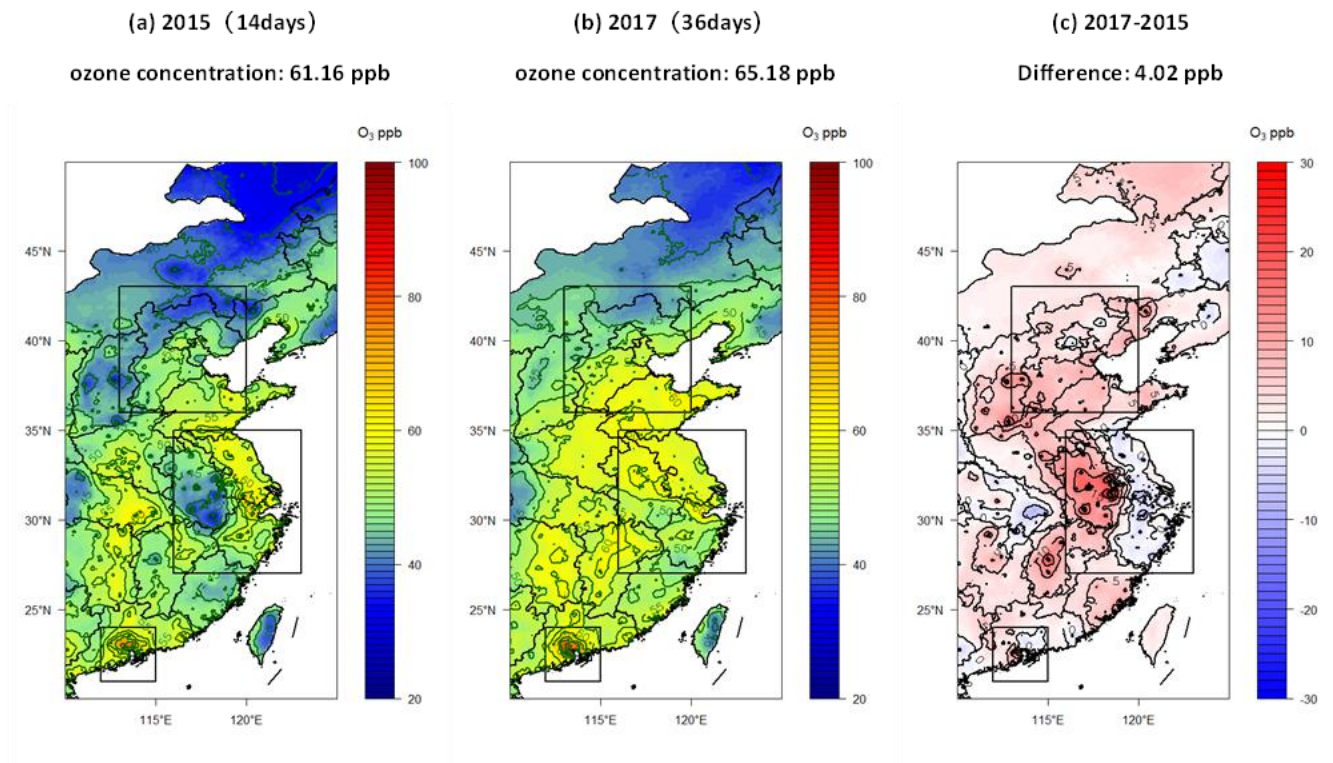
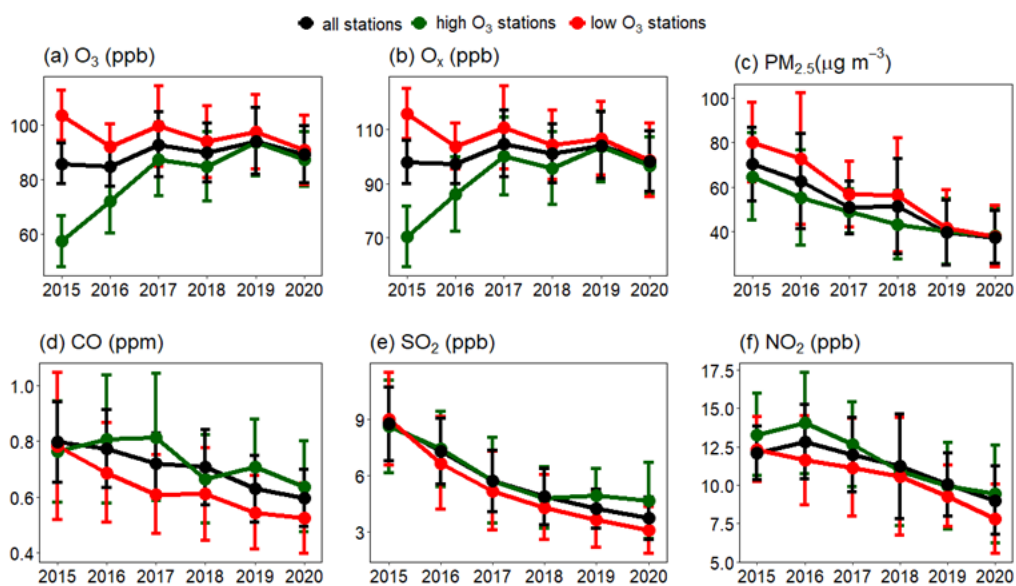
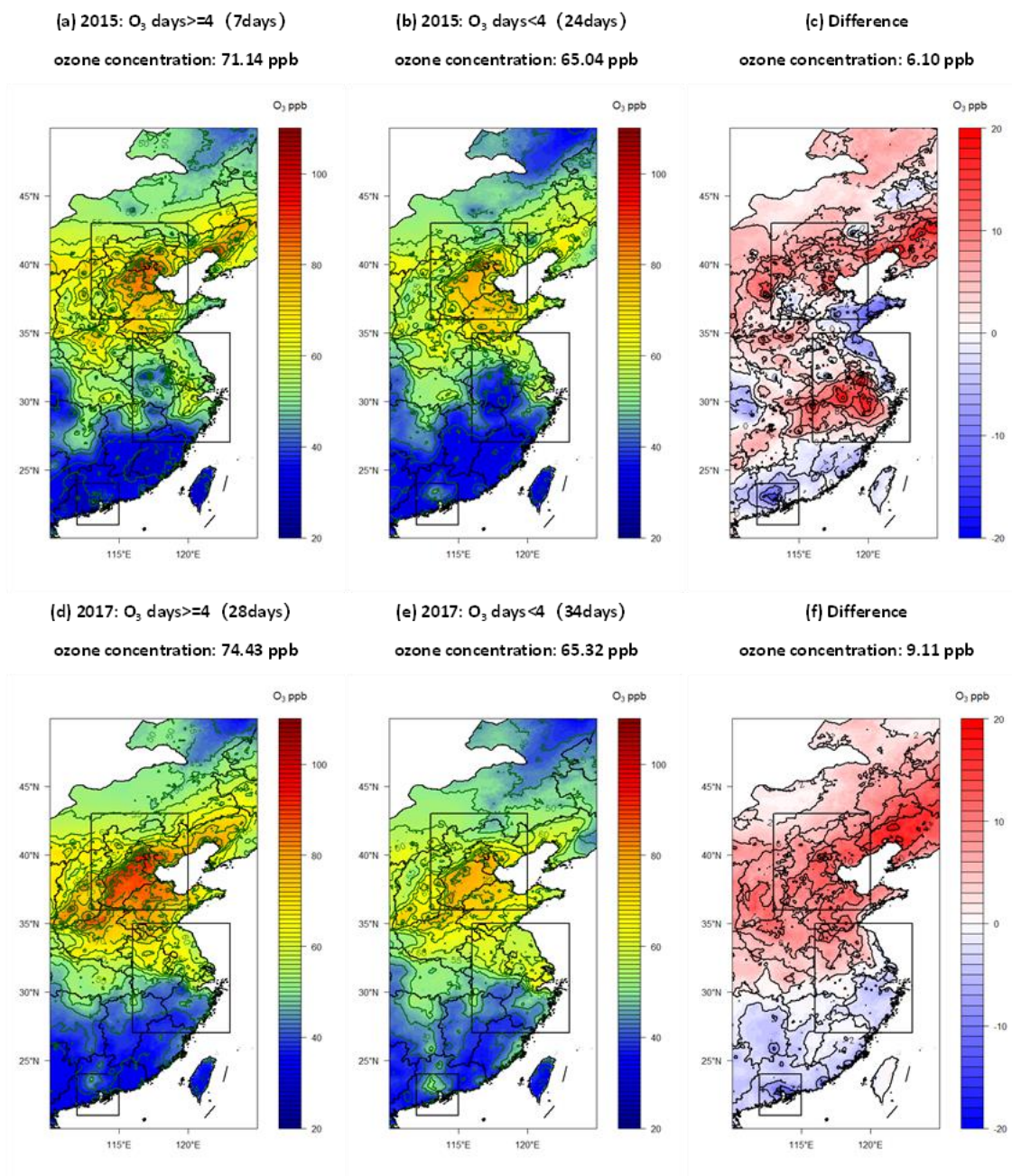


Figure 7: Same as Figure 5 except for PRD.



640 **Figure 8: Annual mean concentrations of maximum daily 8-hour average O<sub>3</sub> in BTH during O<sub>3</sub>-exceeding days for all stations (black), high O<sub>3</sub> stations (red) and low O<sub>3</sub> stations (green) (a), same as (a) except for Ox (b), PM<sub>2.5</sub> (c), CO (d), SO<sub>2</sub> (e), NO<sub>2</sub> (f).**





645 **Figure 9: Spatial distribution of daily mean MDA8 O<sub>3</sub> of O<sub>3</sub>-exceeding days in BTH for O<sub>3</sub> episodes with four or more consecutive O<sub>3</sub>-exceeding days in 2015 (a), O<sub>3</sub> episodes with less than four consecutive O<sub>3</sub>-exceeding days in 2015 (b), and (a minus b) (c); (d, e and f) are the same as (a, b and c), respectively, except for 2017.**



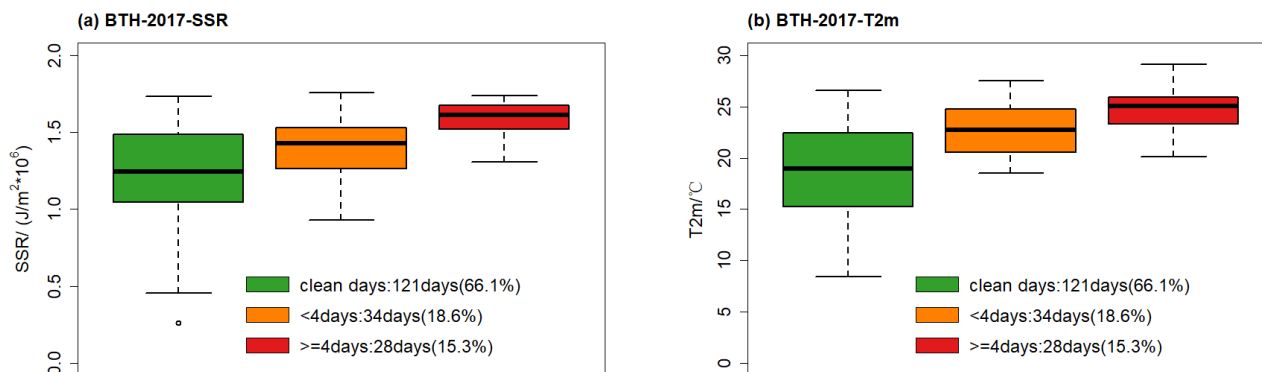
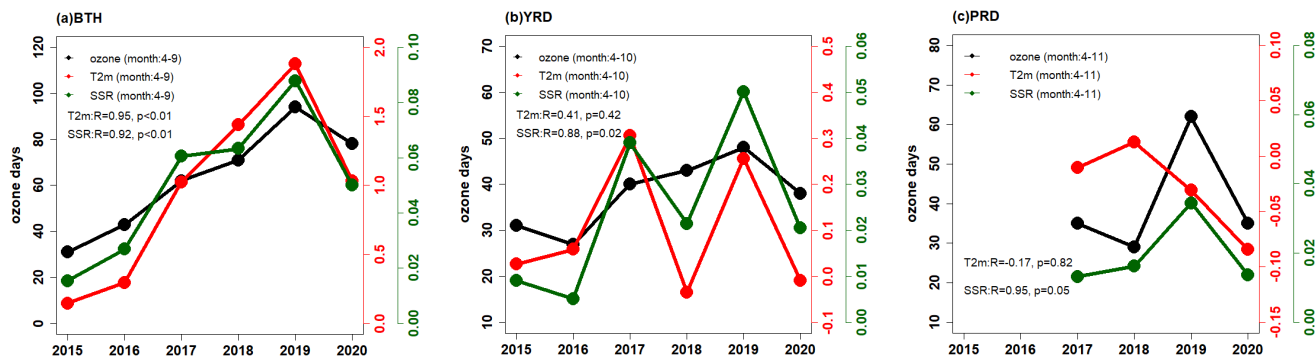
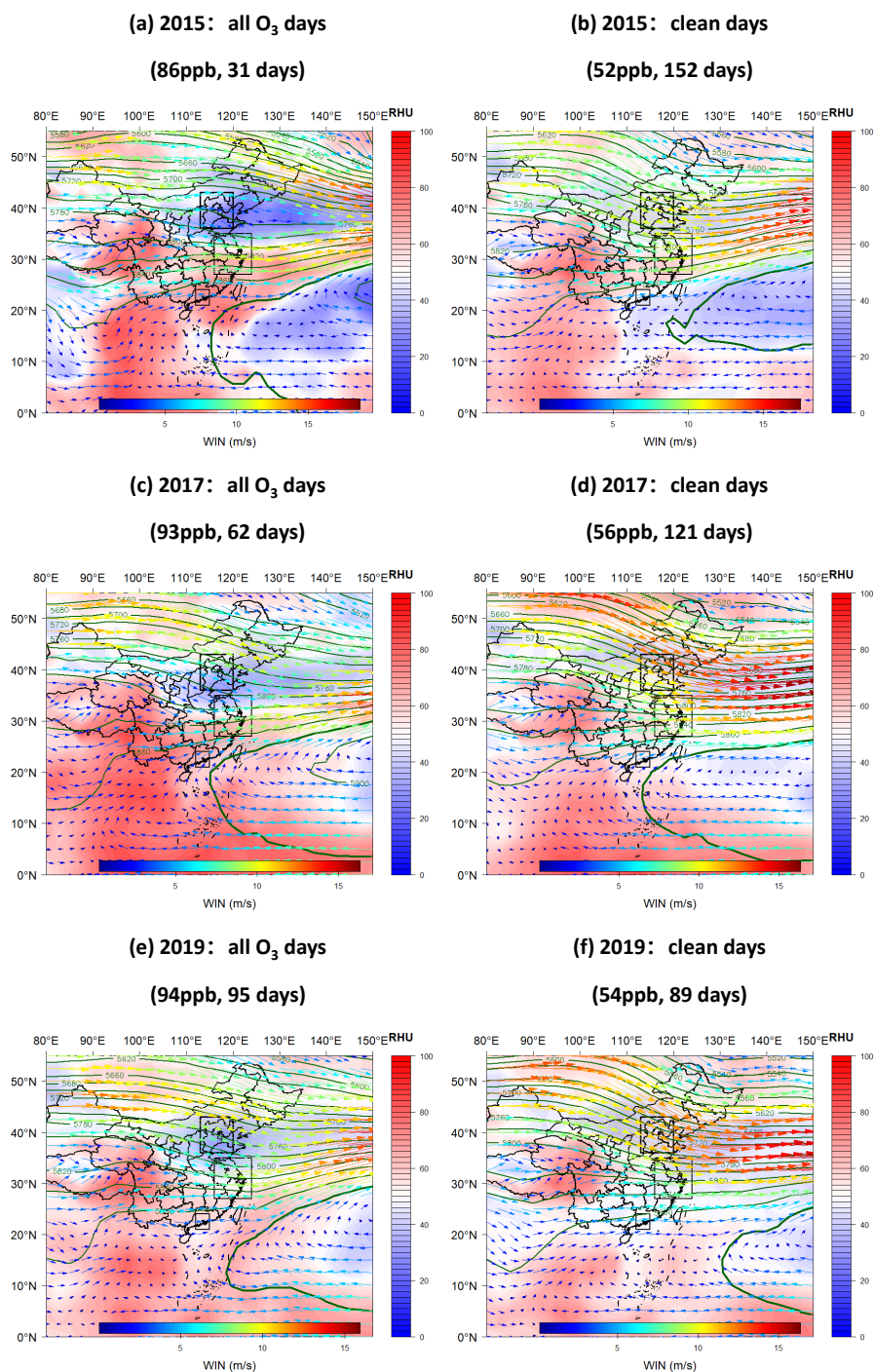


**Figure 10: Surface solar radiation (SSR) (a) and temperature (T2m) (b) in BTH in April–September 2017 for four episodes with four or more consecutive O<sub>3</sub>-exceeding days (red), clean days (non-O<sub>3</sub>-exceeding days) (green) and O<sub>3</sub> episodes with less than four consecutive O<sub>3</sub>-exceeding days (orange).**

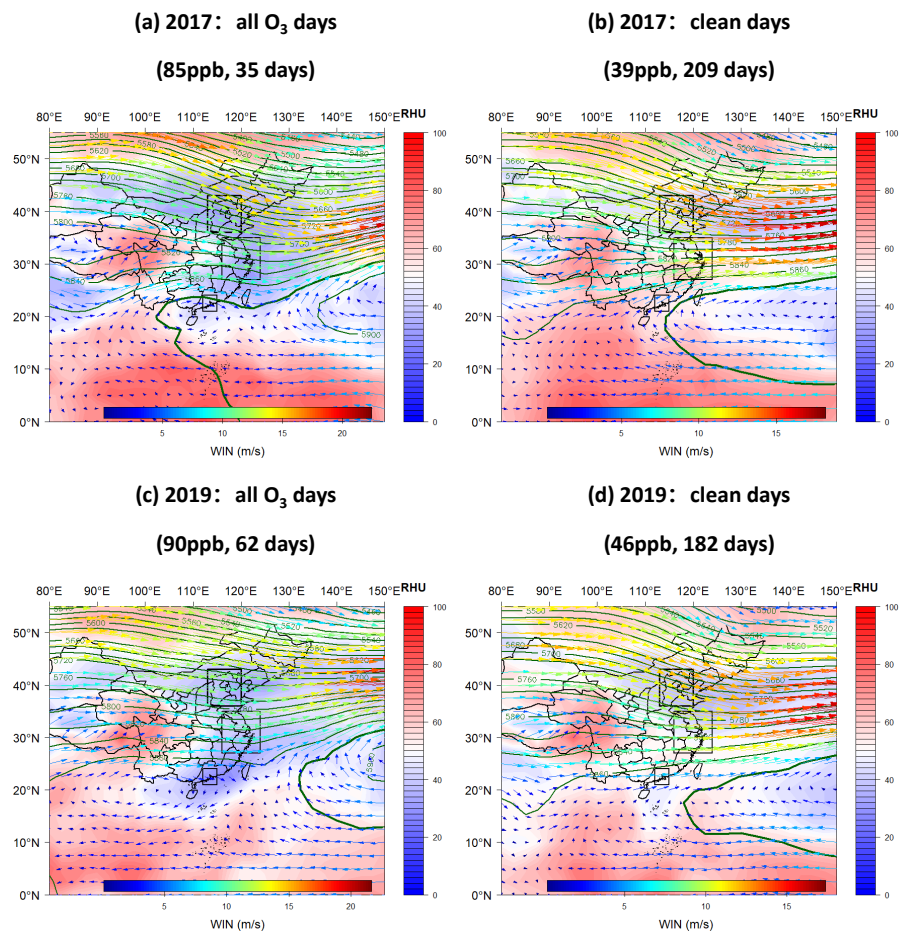


650

**Figure 11.** Correlations among annual O<sub>3</sub>-exceeding days, surface solar radiation (SSR) and temperature (T2m) in BTH (a), YRD (b) and PRD (c).



655 **Figure 12: Composite 500 hPa geopotential height contours, humidity and winds in BTH in April-September for O<sub>3</sub>-exceeding days in 2015 (a), clean days in 2015 (b), O<sub>3</sub>-exceeding days in 2017 (c), clean days in 2017 (d), O<sub>3</sub>-exceeding days in 2019 (e) and clean days in 2019 (f).**



660 **Figure 13: Composite 500 hPa geopotential height contours, humidity and winds in PRD in April–November for O<sub>3</sub>-exceeding days in 2017 (a), clean days in 2017 (b), O<sub>3</sub>-exceeding days in 2019 (c), clean days in 2019 (d).**